EXPERIMENTAL AND MODEL BASED INVESTIGATION OF PERIOD DOUBLING PHENOMENON IN HUMAN STEADY STATE VISUAL EVOKED POTENTIAL RESPONSES

A THESIS SUBMITTED TO

THE GRADUATE SCHOOL OF ENGINEERING AND SCIENCE

OF BILKENT UNIVERSITY

IN PARTIAL FULFILLMENT OF THE REQUIREMENTS FOR

THE DEGREE OF

MASTER OF SCIENCE

IN

ELECTRICAL AND ELECTRONICS ENGINEERING

By

Yiğit Tuncel

July 2018

EXPERIMENTAL AND MODEL BASED INVESTIGATION OF PERIOD DOUBLING PHENOMENON IN HUMAN STEADY STATE VISUAL EVOKED POTENTIAL RESPONSES

By Yiğit Tuncel

July 2018

We certify that we have read this thesis and that in our opinion it is fully adequate, in scope and in quality, as a thesis for the degree of Master of Science.

Yusuf Ziya İder(Advisor)

Hacı Hulusi Kafalıgönül

Yeşim Serinağaoğlu Doğrusöz

Approved for the Graduate School of Engineering and Science:

Ezhan Karaşan
Director of the Graduate School

ABSTRACT

EXPERIMENTAL AND MODEL BASED INVESTIGATION OF PERIOD DOUBLING PHENOMENON IN HUMAN STEADY STATE VISUAL EVOKED POTENTIAL RESPONSES

Yiğit Tuncel
M.S. in Electrical and Electronics Engineering
Advisor: Yusuf Ziya İder
July 2018

Objective. Previous human Steady State Visual Evoked Potential (SSVEP) experiments have yielded different results regarding the range of stimulus frequencies in which Period Doubling (PD) behavior is observed. There also is lacking information about the consistency and repeatability of the occurences of subharmonic oscillations. The neural mechanism of such oscillations have also not been explored. To elaborate these rather unknown aspects of the PD behavior in SSVEP responses, an experimental and model based approach has been taken. ***Approach.*** The experimental side of the study aims at obtaining experimental and statistical data regarding the frequency range of PD generation and also investigates other characteristics of PD. In two sets of experiments, seven subjects were presented a sinusoidal flickering light stimulus with frequencies varying from 15 Hz to 42 Hz. To observe the short term repeatability in PD generation, another set of 5 successive experiments performed on five subjects with 10-minute breaks in between. To obtain the SSVEP responses, filtering, signal averaging and Power Spectral Density (PSD) estimation were applied to the recorded EEG. From the PSD estimates, Subharmonic Occurrence Rates (SORs) were calculated for each experiment and were used along with ANOVA for interpreting the outcomes of the short term repeatability experiments. The model based side of the study aims at explaining the observed phenomena in mathematical terms. For this purpose, Robinson's Corticothalamic Model was implemented in both C and Simulink. The experimental procedure was reanimated on the model and the subharmonic generation in the model depending on different values for parameters was observed. The feedback loop that is responsible for the generation of subharmonic components was identified in the model, and this loop was isolated from the rest of the model and further analyzed with a describing function approach. ***Main***

Results. The experimental results showed that although fundamental (excitation frequency) and second harmonic components appear in almost all SSVEP spectra, there is considerable inter-subject and intra-subject variability regarding PD occurrence. PD occurs for all stimulus frequencies from 15 Hz to 42 Hz when all subjects are considered together. Furthermore, the statistical analyses of short term repeatability experiments suggest that in the short term, PD generation is consistent when all frequencies are considered together but for a single frequency significant short term differences occur. There also is considerable variation in the ratio of subharmonic amplitude to fundamental amplitude across different frequencies for a given subject. The modelling results showed that the subharmonic oscillations in the model are of resonance nature and that they can be obtained virtually in any frequency interval depending on the values of the parameters in the system. The intra-thalamic feedback loop in the model is identified to be the potential source of subharmonic oscillations in the system output. When isolated from the rest of the model and examined by itself, it has been found that this feedback loop can show a resonance phenomenon at the subharmonic frequency. By deriving a set of equations containing the necessary conditions for this resonance phenomenon, a semi-analytical method by which one can find the existence of these oscillations has been developed. ***Significance.*** From the experimental studies, important results and statistical data are obtained regarding PD generation. Our results indicate that modelling studies should attempt to generate PD for a broader range of stimulus frequencies by adjusting the parameter values. It is argued that SSVEP based BCI applications would likely benefit from the utilization of subharmonics in classification. Our modelling study is the first to investigate the source of subharmonic oscillations on a mathematical brain model. An experimental verification of the potential origin of such oscillations, which was identified to be the intra-thalamic loop, would be an important work. The proposed semi-analytical method could potentially be used to speed up a future parameter sweep study. We observed that in the current model alpha oscillation and subharmonic oscillations are in some way interrelated and they can not be generated together for any stimulation frequency. This is referred to as alpha entrainment, and is visible only for some stimulation frequencies in experimental results. Thus, we claim that the model is insufficient in explaining the PD phenomenon in SSVEP responses.

Keywords: Steady State Visual Evoked Potential, SSVEP, Period Doubling, Subharmonic, Harmonic, Nonlinear, EEG, Brain, Model, Corticothalamic, BCI.

ÖZET

İNSAN DURAĞAN HAL GÖRSEL UYARILMIŞ POTANSİYEL TEPKELERİNDE PERİYOT KATLANMA OLGUSUNUN DENEYSEL VE MODEL BAZLI İNCELENMESİ

Yiğit Tuncel
Elektrik ve Elektronik Mühendisliği, Yüksek Lisans
Tez Danışmanı: Yusuf Ziya İder
Temmuz 2018

Amaç. Literatürdeki İnsan Durağan Hal Görsel Uyarılmış Potansiyel (DHGUP) deneyleri, Periyot Katlanması (PK) davranışının gözlemlendiği uyaran frekanslarının aralığı ile ilgili farklı sonuçlar vermiştir. Ayrıca, altharmonik salınımların oluşumunun tutarlılığı ve tekrarlanabilirliği hakkında bilgi eksiktir. Bu tür salınımların altında yatan nöral mekanizma da araştırılmamıştır. DHGUP yanıtlarında PK davranışının bu bilinmeyen yönlerini anlamak için, deneysel ve model bazlı bir yaklaşım ele alınmıştır. ***Yaklaşım.*** Araştırmanın deneysel tarafı, PK davranışının frekans aralığı ile ilgili deneysel ve istatistiki veriler elde etmeyi ve ayrıca PK ile ilgili diğer bazı özellikleri araştırmayı amaçlamaktadır. Yedi deneğe, iki aşamalı bir deneyde, 15 Hz ile 42 Hz arasında değişen frekanslarda sinüzoidal yanan bir ışık uyarısı sunulmuştur. PK oluşumundaki kısa süreli varyasyonları gözlemlemek için, beş denek üzerinde aralarında 10 dakikalık aralar bırakılarak 25-35 Hz aralığını kapsayan 5 ardışık deney daha yapılmıştır. Kaydedilen EEG'ye DHGUP yanıtlarını elde etmek için filtreleme, sinyal ortalama ve Güç Spektral Yoğunluk (PSD) tahmini uygulanmıştır. PSD tahminlerinden, her bir deney için Altharmonik Oluşum Oranları (SOR) hesaplanmıştır. Bu nicelikler kısa dönem tekrarlanabilirlik deneylerinin sonuçlarını yorumlamak için varyans analizi (ANOVA) ile incelenmişlerdir. Araştırmanın model tabanlı tarafı, gözlemlenen fenomenleri matematiksel olarak açıklamayı amaçlamaktadır. Bu amaçla, Robinson'un Kortikotalamik Modeli hem C hem de Simulink'te uygulanmıştır. Deney prosedürü model üzerinde yeniden canlandırılmıştır ve farklı parametre değerlerine bağlı olarak modeldeki altharmonik oluşumu incelenmiştir. Modelde altharmonik bileşenlerin üretilmesinden sorumlu olan geri besleme döngüsü tanımlanmış ve bu döngü modelin geri

kalanından izole edilerek tanımlayıcı fonksiyon yaklaşımıyla analiz edilmiştir. ***Ana sonuçlar.*** Deneysel sonuçlara göre, temel (uyarım frekansı) ve ikinci harmonik bileşenleri hemen hemen tüm DHGUP spektrumlarında görünse de, PK oluşumuna ilişkin dikkate değer bir denek içi ve denekler arası değişkenlik mevcuttur. Tüm denekler birlikte ele alındığında, PK 15 Hz ile 42 Hz arasındaki tüm uyaran frekansları için görülmektedir. Ayrıca, kısa dönemli tekrarlanabilirlik deneylerinin istatistiksel analizleri, tüm frekanslar birlikte ele alındığında altharmonik üretiminin tutarlı olduğunu ancak tek bir frekans için önemli kısa vadeli farklılıkların meydana geldiğini göstermektedir. Aynı zamanda, herhangi bir denek için farklı frekanslardaki temel komponentin genliğinin altharmonik genliğine oranında önemli bir varyasyon mevcuttur. Modelleme sonuçları, modeldeki altharmonik salınımların rezonans doğasına sahip olduğunu ve sistemdeki neredeyse tüm parametrelerin değerlerine bağlı olarak herhangi bir frekans aralığında elde edilebildiğini göstermiştir. Modeldeki intra-talamik geri besleme döngüsünün, sistem çıktısındaki altharmonik salınımın potansiyel bir kaynağı olduğu tespit edilmiştir. Modelin geri kalanından izole edilip kendi başına incelendiğinde, bu geri besleme döngüsünün, altharmonik frekansta bir rezonans fenomeni gösterebileceği bulunmuştur. Bu rezonans fenomeni için gerekli koşulları içeren bir denklem kümesinin türetilmesiyle, bu salınımların varlığını bulabilen yarı analitik bir yöntem geliştirilmiştir. ***Önemi.*** Deneysel çalışmalardan PK üretimi ile ilgili önemli sonuçlar ve istatistiksel veriler elde edilmiştir. Sonuçlarımız, modelleme çalışmalarının daha geniş bir uyaran frekans aralığı için PK üretmesinin doğruluğunu göstermektedir. DHGUP tabanlı BBA uygulamalarının, sınıflandırma aşamasında altharmonik frekansların kullanımından yarar sağlayacağı önerilmektedir. Modelleme çalışmamız, bir matematiksel beyin modelindeki altharmonik salınımların kaynağını araştıran ilk çalışmadır. Bu salınımların potansiyel kaynağı olarak tanımlanan intra-talamik döngünün deneysel olarak doğrulanması önemli bir çalışma olacaktır. Gelecekte yapılacak bir parametre süpürme çalışması önerilen yarı analitik yöntemden yararlanabilir. Mevcut modelde alfa salınımının ve subharmonik salınımların bir şekilde birbiriyle ilişkili olduğu ve herhangi bir uyarım frekansı için birlikte oluşturulamayacağı gözlemlenmiştir. Bu olay alfa sürüklenmesi (alpha entrainment) olarak adlandırılmakta ve deney sonuçlarında sadece bazı uyarım frekansları için görünmektedir. Bu nedenle, modelin SSVEP yanıtlarındaki PK davranışını açıklamakta yetersiz olduğu önerilmektedir.

Anahtar sözcükler: Durağan Hal Görsel Uyarılmış Potansiyel Tepkeleri, DHGUP,

Periyot Çiftlenmesi, Altharmonik, Harmonik, Nonlineer, EEG, Beyin, Model, Kortikotalamik, BBA.

Acknowledgement

I would like to express my deepest gratitude to my advisor Prof. Dr. Yusuf Ziya İder for the continuous support and mentorship throughout my MSc study and related research. This work would not have been possible without his valuable guidance, profound belief and extensive knowledge. It has been a great pleasure to know him and work with him.

I would like to express my appreciation to my committee, for reviewing my work, giving helpful advice, and sharing their constructive criticism.

I would also like to thank to Asst. Prof. Hacı Hulusi Kafalıgönül and Dr. Utku Kaya for their close interest and support throughout my MSc study.

I am grateful to Prof. Dr. Ömer Morgül for his valuable guidance and advices on my research.

I want to thank Mürüvet Parlakay for her help on administrative works.

I am thankful to Ufuk Tufan, Onur Bostancı, and especially to Ergün Hırlakoğlu for their technical and practical knowledge and friendly approach.

My parents and my little sister, I cannot thank you enough for making me the person I am today. Without your support, guidance and love, I wouldn't have achieved this and learned how to succeed. All the support you have provided me over the years was the greatest gift anyone has ever given me.

Finally, I would like to thank to my best friend and colleague Toygun Başaklar for all the good times we had. I admire his formidable practicality and attention to detail, and most importantly, I put great value in his friendship. I also want to thank to the very valuable past and present members of EMTP and BCI Group for being great friends to me.

I want to acknowledge The Scientific and Technological Research Council of

Turkey (TÜBİTAK) for providing financial support under Grant 116E153 during my MSc studies.

Contents

List of Figures

List of Tables

Chapter 1

Introduction

1.1 Motivation and Objective

Steady State Visual Evoked Potentials (SSVEPs) are oscillatory potentials elicited in electroencephalogram (EEG) in response to periodic light stimulation [1, 2]. SSVEP responses have been widely used in engineering applications such as Brain-Computer Interfaces (BCIs) [3] and cognitive and clinical research [4, 5]. These responses are characterized as oscillations at the stimulus frequency as well as its harmonics and subharmonics [2, 5, 6, 7]. Particular interest has been shown to understand some of the nonlinear dynamics SSVEP responses have, including harmonics generation, alpha entrainment to stimulus frequency and frequency mixing [2, 5, 6, 8, 9, 10, 11]. However, the generation of subharmonics, which have been observed by several researchers [6, 12, 13, 14], has not received much attention and need to be better understood. (Throughout the thesis, "subharmonic frequency" is used to refer to half of the stimulus frequency, and "period doubling" is used to refer to the generation of subharmonic frequency.)

We refer to the generation of the first subharmonic component as Period Doubling (PD) Phenomenon, i.e. given a flickering stimulus with a frequency of f, we

observe a strong and distinct component at $f/2$ in the EEG spectrum. This phenomenon has been observed in several experimental SSVEP studies for different frequency ranges: Herrmann's findings indicated that subharmonic generation may occur for stimulation frequencies in 15-30 Hz range [6]. Crevier and Meister reported subharmonic components for stimulus frequencies between 30-70 Hz [12]. Tsoneva et al. have observed subharmonic generation in the 40-60 Hz stimulus frequency range [13].

There is considerable ambiguity on the subject of period doubling in SSVEP experiments in the literature regarding at which stimulation frequencies period doubling occurs and how consistent this occurrence is. This ambiguity also holds back the investigators who aim at developing realistic cortex simulation models. Besides, an inclusive experiment that investigates the nonlinear behaviors of SSVEPs induced by a purely sinusoidal stimulus is absent. Therefore, one can claim that there is need for additional experimental data to clarify the various issues related to subharmonic generation in SSVEP responses.

Despite many years of research in this field, mechanisms that depict such nonlinear interactions under periodic stimulus are still unresolved [5]. In more recent years, modeling studies have started to emerge [14, 15, 16], that aim to explore such mechanisms. However, none of the mentioned studies identified a mathematical explanation to the mechanisms underlying such components. Considering all the previous work, it is arguable that subharmonic components in SSVEP responses could be a focus of new theoretical studies.

1.2 Scope of the Study

With the ideas and motivations presented in Motivation and Objective section, this study approaches the PD phenomenon in SSVEP responses from two aspects: (i) Experimental investigation of the PD phenomenon and (ii) Model based investigation of the PD phenomenon. In part (i), we have generated an FPGA based

light stimulus as part of our experimental procedure and employed this procedure to conduct SSVEP experiments on 9 subjects. These experiments focused on gathering experimental and statistical data regarding subharmonic responses. We have compared our findings with the findings of other researchers. We have also identified and explained various characteristics of the period doubling behavior. In part (ii), we utilized a fairly recent corticothalamic model to explore the possible mechanisms underlying these experimentally observed phenomena. For this purpose, we employed Robinson's Corticothalamic Model, analyzed its PD behaviour in response to a sinusoidal drive and also compared its predictions with our experimental findings. We have used nonlinear feedback system approaches to understand and explain how these oscillations are generated in the mathematical sense.

1.3 Organization of the Thesis

This thesis consists of five chapters:

In chapter 2, background information and core knowledge regarding Steady State Visual Evoked Potentials, PD in feedback systems, and models of the brain is provided. Beginning from the very basics, an explanation of the importance of EEG in studying human brain is given. Then, the notion "Visual Evoked Potential", VEP, is explained and is further boiled down to Steady State Visual Evoked Potentials. Next, fundamental theories about subharmonic generation in feedback systems are given. An analysis method called "Describing Function" analysis is shared with the reader. Lastly, the general approach of quantitative modeling of the brain is explained, from the more vague ensemble approach to neural mass models and furthermore to larger scale brain network models and neural field models. The information in this part is perseveringly useful throughout the text.

In chapter 3, the experimental approach to obtain statistical data about subharmonic components in SSVEP responses is elucidated. First, a recapitulation

of earlier experimental studies in which PD phenomenon are present is provided. Then, our experimental procedure and data analysis techniques are presented to the reader. The chapter proceeds with documenting the results of the experiments and concludes with relevant discussion of these results.

In chapter 4, the model based approach to obtain a mathematical explanation for the underlying mechanisms of subharmonic components in experimental SSVEP studies is detailed. First, a brief compilation of earlier modeling studies with similar scope is shared with the reader. Then, the employed corticothalamic model is mathematically constructed with very simple narration that presents many important points and assumptions in the modeling work. The effects of the parameters in the model to PD behavior is analyzed and explained in this chapter. A possible origin for the subharmonic components are presented to the reader and lastly, the outcomes of the modeling study are further evaluated and discussed.

In chapter 5, results obtained in chapters 3 and 4 are summarized and these results are evaluated and compared. It is also discussed whether the model that we have employed is sufficient in explaining the observed behaviors in SSVEP experiments.

Chapter 2

Background

2.1 Electroencephalogram, Visual Evoked Potentials and Steady State Visual Evoked Potentials

In cognitive and clinical neuroscience, two different types of activity in the brain are generally utilized: (i) electrophysiological activity and (ii) blood flow (hemodynamics). Electrophysiological activity is in the form of current flows inside neurons and between different neurons and neural ensembles. These intracellular and extracellular (intercellular) currents in turn causes a spatial voltage distribution in the whole brain and induces a magnetic field. Magnetoencephalography (MEG) is a method that measures the induced magnetic field while electroencephalography (EEG), electrocorticography (ECOG) and individual neuron recordings are among the most common methods that record the electric field (i.e. potential differences). The hemodynamic activity is the result of oxygen rich blood flow towards active areas (neurons) in the brain. This blood flow causes a change in the oxyhemoglobin to deoxyhemoglobin ratio in the local tissue [17]. Functional Magnetic Resonance Imaging (fMRI) and Near Infrared Spectroscopy are methods that measure and quantify this ratio. Among these methods, EEG is the

most commonly used technique when stimulus driven activity is being considered due to its temporal accuracy, very low equipment cost and safety.

2.1.1 Electroencephalogram (EEG)

EEG is recorded noninvasively through electrodes placed on the scalp. An EEG recording system (generally referred to as an EEG amplifier) consists of electrode(s), amplifier(s) and ADC(s). Usually this system is connected to a computer to store and preferably display the recorded data. In unipolar recordings, there is a "reference" electrode that serves as the reference point for the potential at each electrode site while in bipolar recordings potential difference between any pair of electrodes can be measured. Amplifiers of a typical EEG system have gains in the x10000 range as the recorded potentials typically have amplitudes in microvolts range. The amplified signal then is digitized by a high resolution ADC (typically with 24bit resolution) and is forwarded to the recording computer.

The definition of a recorded EEG signal at each sample point is the potential difference between two electrode sites. This signal is mostly due to the extracellular current flows in the underlying brain structure [18]. Due to many layers between the source of the signal (neurons) and the recording site, EEG is very susceptible to background noise and may include artifacts. The most important precaution to eliminate noisy recordings is to have little electrode/scalp contact potential. This impedance is generally kept below $10k\Omega$ [19], and this is generally achieved by applying conductive gel to the interface between the electrode and scalp. Recent advancements in this area include the so called active electrodes, that have filters/amplifiers on the recording site. Also, gel-less "dry" electrodes are being developed to remove the need to the mentioned conductive gel [20, 21]. In any case, participants/subjects should be warned for being stationary (especially head and shoulder motions should be avoided) during an experimental study and necessary precautions (distance to power lines, cable length, etc.) should be taken into consideration when an experiment is being designed.

EEG signal is divided into five frequency bands, and each of these bands are

associated to a particular state of mind or action: delta (δ), theta (θ), alpha (α), beta (β), and gamma (γ). Delta band includes the frequencies 0 to 4 Hz. These components are generally observed during deep sleep state in adults [22]. However, due to being low frequency components, these are generally filtered out along with artifacts caused by slow head and neck movements. Theta band includes the frequencies 4 to 7 Hz. These components are generally observed during meditative states and during cognitive processes such as mental calculation and maze solving [23, 24, 25, 26]. During awake state, theta band components tend to not exist in healthy human adults. Alpha band includes the frequencies in the 8 to 12 Hz interval. They are primarily associated with visual processing and are very strongly observable in the recordings made from occipital lobe of the brain where primary visual areas reside (back of the head) [27, 28]. When eyes are closed alpha band power increases significantly. Alpha components also tend to disappear with increasing mental effort) [29, 30]. Beta band includes the frequencies 12 to 30 Hz. They are linked with motor activities and are mostly observed in frontal and central part of the brain where motor areas reside. They tend to suppress during movement or imagination of movement (motor imagery) [31]. Gamma band includes frequencies from 30 to 100 Hz (typically EEG spectrums are not observed beyond 100 Hz). A clear and strict association of gamma band components with a state or activity is not as prominent as other bands. There are studies that correlate gamma band oscillations to certain motor functions and perception of visual and auditory stimuli [32, 33, 34, 35, 36]. Gamma band is generally free of artifacts (except electromyograph (EMG) artifacts which are easily understandable due to EMG's very high amplitude) and components in this range have relatively low power in the frequency domain. This makes this range suitable for studies including frequency domain investigation.

Activities in these frequency bands may be altered with exogenous effects (external sensory stimuli) as well as endogenous effects (internal cognitive processes) [8]. These alterations are called event related potentials (ERPs). ERPs are defined as "the general class of potentials that display stable time relationships to a definable reference event" in [37]. The exogenously induced ERPs are termed as sensory evoked potentials (SEPs). SEPs are EEG signals that

are phase-locked to the stimulus applied to a sensory organ [38]. As they are phase-locked to the stimulus, their appearance can be made more prominent by applying the stimulus many times and averaging the recorded EEGs from the time onsets of the stimuli. A specific type of SEP is the visual evoked potentials (VEPs) which are changes in the EEG in time following a visual stimulus, most commonly a light flash [39].

2.1.2 Visual Evoked Potentials (VEPs)

VEPs are brain activity changes in the visual cortex induced by a visual stimulus [2]. They can be separated into three categories according to their mechanism of generation [40]: (i) form of the stimulus, (ii) frequency of the stimulus and (iii) type of the stimulus. The first category separates VEPs by the form of the stimulus, generally as flash induced VEPs or pattern induced VEPs. A flash induced VEP (or briefly a flash VEP) is obtained when a uniform flash is used as the stimulus. A pattern induced VEP can further be categorized as pattern reversal VEP or pattern on/off VEP. Most commonly a checkerboard grid is used as the pattern in these stimuli. The second category separates VEPs by the frequency of the stimulus, generally as transient VEPs or steady state VEPs. Transient VEPs are the responses of the visual system when the stimulus is brief and suddenly changes [41]. In contrast to these, steady state VEPs are obtained in response to a train of such stimuli with a fixed presentation rate [1]. These are termed as steady state since the VEPs in this case are stable oscillations with relatively unchanged amplitude and phase over time [42]. The third category separates VEPs by the type of the stimulus, generally as full field VEPs or part field VEPs. If the stimulus stimulates the whole visual field, the obtained VEP in this case is a full field VEP and similarly, if it stimulates half of the visual field or a part of the visual field, the obtained VEPs are called half field VEPs and part field VEPs respectively.

2.1.3 Steady State Visual Evoked Potentials (SSVEPs)

Steady State Visual Evoked Potential is the evoked response that has a periodic time course induced by a stimulus which is modulated periodically as a function of time. As these responses are periodic, they are typically analysed in the frequency domain instead of the time domain, unlike other kinds of VEPs and ERPs. The frequency content of a typical SSVEP response contains peaks at frequencies that are directly related to the stimulation frequency (f). These peaks are generally at the fundamental frequency (f), harmonics of this frequency (2f, 3f and rarely higher order harmonics) and subharmonic of this frequency (f/2) [5]. These peaks are very narrow band peaks with high amplitudes and are easily discernible from the background spectrum [2]. In addition to the amplitude of these SSVEP peaks, response phase is another parameter that is meaningful for SSVEPs [8]. The phase value is made up of processing/integration times and propagation delays in the retina, between the retina and the cortex, and in the cortex. As stated above, SSVEPs contain harmonics and subharmonics in their spectrum even if the stimulus is a pure sinusoidal light modulation (i.e. it has no other component in its spectrum other than the frequency of interest, f). This is due to the nonlinearity of the visual system. If the visual system was linear, the frequency spectrum of the SSVEP response would only include a peak at the stimulation frequency, possibly with modulated amplitude and phases. However, the presence of nonlinearly generated components (harmonic and subharmonic components) shows that the nature of the visual system is of nonlinear type.

Real SSVEP recordings are, as should be expected, highly contaminated by noise. This noise may be measurement noise and artifacts, but more importantly, it is generally in the form of additive EEG noise [43]. Even if spectral content is less affected than temporal content by the former noise types, background EEG activity may disrupt the spectral content significantly enough to render any analysis unhealthy. For example, the person may have large alpha range oscillations, yielding high power at alpha band in the frequency domain. This would affect an SSVEP study with a stimulation frequency in the alpha range (8-12 Hz). Luckily, SSVEP responses are narrow band (they appear as sharp peaks)

provided that the recording is long enough to have sufficient spectral resolution. This allows for averaging, a very effective pre-processing step in the analysis of SSVEP signals, as random additive background EEG noise is canceled out during averaging. This is possible because SSVEP responses are in phase with the stimulus and do not cancel out during averaging.

The stimulus frequency range that depict SSVEP responses is generally accepted to be 3-50 Hz interval. However, there are studies that challenge both the upper and lower boundaries of this range, so the best (and current) practice is not to define any limit or range [8].

SSVEP responses are used in many different applications, including cognitive neuroscience (visual attention, binocular rivalry, working memory, alpha range), clinical neuroscience (neurodegenerative disorders, schizophrenia, ophthalmic pathologies, migraine, depression, autism, epilepsy, etc.), and engineering in the form of Brain Computer Interfaces [5]. SSVEPs can be recorded with many different imaging modalities (individual neuron recordings, ECOG, EEG, MEG, fMRI and many others) but EEG remains to be the most common method owing to its good temporal resolution, low cost and portability [5].

In light of the above information, SSVEPs can be very briefly defined with the following words: "SSVEPs are evoked responses induced by flickering visual stimuli. SSVEPs are periodic, with a stationary distinct spectrum showing characteristic SSVEPs peaks, stable over time SSVEPs are better observed in the frequency or time–frequency domains." [5].

2.2 Nonlinear Systems, Subharmonic Oscillations and Describing Function

2.2.1 Nonlinear Systems

A linear system obeys the "principle of superposition". This principle states that once the responses to a set of input signals are known, then response to any of kind combination of these inputs can be found with superposition of each individual response. In mathematical terms, if inputs $i_1(t)$ and $i_2(t)$ yield responses $r_1(t)$ and $r_2(t)$ respectively, then for all a and b, an input of the form $ai_1(t) + bi_2(t)$ yields the response $ar_1(t) + br_2(t)$. This principle allows for the transfer function analysis of linear systems because once the response to a set of sinusoidals with different frequencies are known, the system response to any combination of these is inherently known.

Nonlinear systems, on the other hand, do not obey this principle. This makes the analysis and study of these systems a challenging task. This is because knowing the response to a kind of input $x(t)$ does not necessarily contribute to knowing the response to another kind of input that includes $x(t)$. There is no guarantee $x(t)$ and $x(t)+\epsilon$ will generate similar responses, they may yield entirely different responses. This lack of generalization brings the need to analytically find or numerically compute the response of the system to any kind of input and makes the analysis of nonlinear systems a tedious task. However, many feedback systems include nonlinear elements and studying these elements has been an indispensable task for researchers [44].

2.2.2 Subharmonic Oscillations in Nonlinear Systems

A very important property of linear systems is that they pass the frequency content of the input signal to output, possibly with different amplitudes and phases, without introducing any new frequency. In other words, if a linear is system is

excited with a sinusoidal input with a frequency ω_i (say $a\sin(\omega_i t + \phi_1)$), the output will be a sinusoid of the form $b\sin(\omega_i t + \phi_2)$ for any ω_i. Nonlinear systems, on the other hand, usually yield a totally different frequency content at the system output. A sinusoidal input to the system does not necessarily yield a sinusoidal response at the output as in the case of linear systems. Most commonly, frequency content of the output signal contains components that are multiples of the input frequency (kf where $k = 1, 2, 3, ...$). These are termed as the "harmonic components". Not as commonly as these, some nonlinear systems depict what we call as the "subharmonic generation". In this case, frequency content of the output signal contains components that are submultiples of the input frequency ($1/nf$ where $n = 2, 3, ...$). We refer the generation of the subharmonic component when n=2 as the "period doubling" phenomenon. The component that corresponds to k =1 is referred to as the fundamental frequency component, meaning the input frequency. The following harmonic components where $k = 2, 3, ...$ are referred to as second harmonic component, third harmonic component and so on. The subharmonic components where $n = 2, 3, ...$ are referred to as first subharmonic component, second subharmonic component and so on.

Due to the resonant nature of the subharmonic components, these oscillations are of large amplitude and dominate system output. This causes the system output to be entirely different from the sinusoid at the input. This significant difference has been considered unwanted in most feedback control systems (such as in loudspeakers, servo motors, etc.) and for this reason, this phenomenon had been investigated to understand the conditions under which these oscillations may happen.

2.2.3 Describing Function Analysis

Linear systems are analyzed in the frequency domain through transfer functions. There had been a search for a similar tool for nonlinearities, such that the frequency response of a nonlinearity is defined by an equation which is compatible with transfer functions of the linear components in the system. These equations

are termed as the "describing function" of a nonlinearity and they approximate the effects of a nonlinear component on the frequency content of its input.

Recent advances in computing power allows for numerical computation of these describing functions. Originally, these functions were analytically found (for some nonlinearities these could not be found due to integrals being indefinite). For example, for polynomial nonlinearities describing functions can be analytically expressed with the help of trigonometric identities [45]. But for exponential nonlinearities this is not possible [44]. A brief explanation of the procedure to calculate the describing function of a nonlinearity N(x) is given below [46] (Wang Analyzing Oscillators using DFs):

1) Set $x(t) = A_k sin(2\pi kft + \phi_k)$ as the input to $N(x)$ where $k = 1/2, 1, 2, 3, ...$ until where the low pass nature of the linear part of system kills of the component with frequency kf.
2) Get output: $y(t) = N(x(t))$.
3) Compute the fourier transform of $y(t)$, get Fourier coefficients at frequencies kf, OR directly compute the fourier coefficients at frequencies kf.
4) Express the components in phasor representation with using the fourier coefficients at each kf (e.g. $B_k e^{j\phi_{Bk}}$ for each kf).
5) Define the describing function of $N(x)$ as $DF(A_k, \phi_k, kf) = B_k e^{j\phi_{Bk}}/A_k e^{j\phi_k}$.

This type of describing function is termed as multi input describing function (MIDF) [44]. As a result, for each frequency of interest we express the effect of the nonlinearity ONLY for a given input. It is important to note that for even the slightest change in A_k or ϕ_k, the process should be repeated and a new DF should be computed. Notice that it is very important that the harmonics in the feedback signal are adequately low pass filtered.

2.3 Quantitative Models of the Brain

The information processing behind many crucial brain functions (e.g. sensory, motor and cognitive functions) is considered to be carried into effect by crowded populations of interconnected neurons [47, 48, 49, 50]. Neurons are the building blocks of the nervous system, in that they are the cells that are responsible for information transfer in the nervous system. This information transfer is explained by concepts rooted upon the membrane potentials of neurons. The resting membrane potential of a neuron is the electrical potential of a neuron's soma/membrane referenced to extracellular space. Temporary changes in the resting membrane potential of neurons due to inputs coming from surrounding (not necessarily spatially next to) neurons through synapses are termed as post-synaptic potentials (PSP). These PSPs, in turn, cause changes in ion concentrations between intracellular and extracellular space through ion channels. This increased difference in ion concentrations between the inside and the outside of the cell causes the PSP to grow further through a positive feedback mechanism, and after a certain level the neuron produces a spike-like voltage waveform. These spikes are called action potentials (APs). APs are considered to be the fundamental elements of inter-neuronal communication, due to the fact that information is identified to be encoded in terms of both the frequency (termed as the firing rate) and timing of APs.

This mechanism behind the generation of action potentials in single neurons was uncovered by a nobel winning Hodgkin-Huxley model (HH model) [51]. The scientists behind the model, Alan Hodgkin and Andrew Huxley, studied neurophysiological recordings taken from the squid giant axon of a longfin inshore squid. The large size of the axon allowed them to insert electrodes and as a result, they managed to express the generation of action potentials in mathematical terms. However, movement, cognition, or other higher level processes are not immediately explainable by such single neuron discoveries [52, 53]. Such processes are thought to arise from interactions of crowded neuronal populations. Moreover, electroencephalography (EEG) reflect the collective activity of such populations consisting of thousands of neurons [54].

There are branches in science where similar observations are present: the large scale system depicts a collective behavior that is not similar to that of the elements in the said large scale system. Research in such fields aims to generate mathematical laws that govern these macroscopic quantities (e.g. magnetic fields or fluid flow). These mathematical laws or models are mostly generated on the grounds of mean field approximation. This approximation is commonly employed in statistical physics [55] and it helps forming an approach to find the stationary solutions of a dynamical system. The objective of the mean field theory is to approximate the effect of all individuals on any given individual by a single averaged effect, thus reducing a "many-body problem" to a "one-body problem". Neuroscience is not an exception to this: mathematical laws or models that explain the behavior of a population of neurons had been investigated through mean field approximation in the last century.

These models [56, 57, 58] are shortly referred to as mean field neural models [55, 59]. Such models, as underlined above, do not explain the AP generation in individual neurons but explain the collective behavior of a crowded population of neurons [60]. Hence, these models are considered to be appropriate for explaining the empirical data gathered by EEG, MEG or fMRI. A wide variety of phenomena, including resting state brain networks and oscillations [61, 62, 63, 64], seizures [65], sleep states [66], etc., that are observed in such imaging techniques were explored in modeling studies (see [59] for more examples).

Mean field neural models, which explain large scale brain dynamics, are based on methods/approaches from areas such as dynamical systems theory, statistical physics and stochastic calculus. The first and principle approach in this regard, in the field of brain modeling, is to consider the activity of an ensemble of neurons often referred to as the "ensemble density approach".

2.3.1 The Ensemble Approach

Ensemble models aim at modeling the dynamics of crowded populations of neurons (in theory, number of neurons is not bounded). It assumes that individual

states of neurons are irrelevant and are uncorrelated (i.e. correlation between two neurons decay as the distance between them increases in a population). According to the Central Limit Theorem (CLT), sum of many uncorrelated random processes, whose probabilistic densities can be in any form, converges to a Normal distribution [55]. This simplification brings along a very important benefit: dimensionality reduction. The activity of the whole population can thus be expressed by a Normal distribution and its linear statistics. In other words, instead of having to consider firing rates or membrane potentials of individual neurons, the activity of the population can be reflected by the mean and variance of the lumped firing rate [67]. The mean of this distribution denotes the response of the population to the aggregated synaptic inputs and the variance of this distribution denotes how rough the effect of random fluctuations in the neuronal level are (i.e. how precisely the ensemble response is represented).

The mathematical representation of the dynamics of such a normally distributed ensemble is achieved through the Fokker-Planck equation (FPE). A step by step derivation of the FPE is present in [55]. Very briefly, an FPE is derived from an ensemble of single neuron models (such as leaky integrate and fire) under diffusion approximation. In essence, the FPE reflects the congregated response of a neural population by calculating a mean firing rate. As the input of the FPE changes, the drifts in the mean and variance of the mean firing rate is recaptured. The reduction from finding responses of thousands of neurons to finding an aggregated response of the same neuronal population is very crucial in modeling studies. In this case, FPE provides a dimension reduction from thousands of degrees of freedom to two variables, the mean and variance of the mean firing rate. For this reason, ensemble approach is often considered to be the take-off point for large scale brain modeling.

2.3.2 Reduction to Neural Mass Models

A further reduction in dimensionality constructs the motivation behind the notion termed as Neural Mass Models (NMMs) [60]. Under the assumption of a strong

coherence in a neural ensemble, it is possible to disregard the variance and model the population dynamics only via the mean activity. This reduces the dimensions from two to one and essentially reduces the number and complexity of underlying mathematical equations which describe the evolution of the mean activity of the neuronal ensemble. Such assumption brings along the definition of a concentrated neural ensemble (very strong coherence), also termed as a point mass (hence the name "neural mass"). In short, the ensemble is replaced with a point neuronal mass and model/substitute the ensemble dynamics by the dynamics of this mass through a set of nonlinear differential equations. This mass-action approach constitutes the heart of NMMs.

In NMMs, we ignore the effect of variance in the membrane potentials within an ensemble on population dynamics. The most prevalent way to make up for this simplification is to use a sigmoidal function (the general form can be seen in equation 2.1) to relate the average membrane potential to population firing rate [60, 68]. In doing so, the variance of the needed relative potential change for the neuron to fire is indirectly modeled. NMMs are most commonly in the form of second order nonlinear differential equations for the average membrane potential of the population:

$$\begin{aligned} &(\frac{1}{\gamma^2}\frac{\partial^2}{\partial t^2} + \frac{2}{\gamma}\frac{\partial}{\partial t} + 1)V = \phi \\ &\phi = S(V) = \frac{\kappa}{1 + \exp(-rV)} \end{aligned} \tag{2.1}$$

Here V denotes the membrane potential and ϕ denotes the average firing rate of the population. γ is a constant that controls the rise time of V in response to ϕ. κ is a coupling constant and r implicitly covers the above mentioned variance in neuron firings. In summary, NMMs can be regarded as special cases of ensemble models, in that they were reduced by only utilizing the mean of the ensemble density and ignoring the variance.

2.3.3 Brain Network Models and Neural Field Models

2.3.3.1 Brain Network Models

NMMs model rather small and local population of neurons, say a cortical column. For larger scale brain modeling, one approach is to couple NMMs with each other in mesoscopic [60, 69] and macroscopic [70] scales. This way, dynamics in of each local neuronal population (each NMM), is governed by its own dynamics, but are also affected indirectly from the activity in other nodes. This indirect coupling is achieved by anatomical connectivity matrices, also referred to as the connectome. Tractography studies aim to uncover a realistic connectome through invasive recordings or by inverse problem formulations on human fMRI data [71, 72]. In short, such large scale discrete brain models are referred to as Brain Network Models (BNMs), and they aim to bridge the gap between models of local neural populations and large scale brain activity.

2.3.3.2 Neural Field Models

BNMs model the large scale cortex at discrete nodes, and uses connectivity matrices that couple the activities at these nodes. Another approach is to model the cortex as a continuum, on which the coupling coefficients decay exponentially with increasing distance [72]. Such continuous field models employ methods used in other complex systems. Most commonly, the differential equations and spatial couplings are provided in the form of a wave equation (a differential equation that includes both temporal and spatial derivatives) [56, 73]:

$$\begin{aligned} &(\frac{1}{\gamma^2}\frac{\partial^2}{\partial t^2} + \frac{2}{\gamma}\frac{\partial}{\partial t} + 1 - r^2\nabla^2)V = (1 + \frac{1}{\gamma}\frac{\partial}{\partial t})\phi \\ &\phi = S(V) = \frac{\kappa}{1 + \exp(-rV)} \end{aligned} \tag{2.2}$$

Here c is the speed of AP propagation, r is the relative distance, $\gamma = c/r$ and

∇^2 is the laplacian. Notice here that average membrane potential and average firing rate are both functions of space and time. A more detailed explanation of these large scale Neural Fields Models can be found in [55].

2.3.3.3 Forward Models

The outcomes of these models do not necessarily model the observed empirical data. There is a need for another model layer that relates the collective response of a model to the data obtained by the employed imaging modality. EEG, for example, is induced by macroscopic extracellular currents. Such models, that explore the relationship between the cortical currents and EEG, are called forward models. The obtained aggregated response of a model (most likely the derivative of the membrane potential) should be fed to a forward model to obtain a result that is equivalent to experimental results. Especially for inverse problem formulations, these forward models remain to be a very important area of research. However, with assumptions made possible by experimental design, the need for forward models is often discarded in modeling studies such as the current study.

Chapter 3

Experimental Investigation of Period Doubling Behaviour in Human SSVEP Responses

3.1 PD in Earlier Experimental Studies

Several researchers have documented PD behavior in their experimental results. Crevier and Meister have investigated the period doubling phenomena under bright full field flickering square wave light stimulus in salamander and human [12]. For humans, both in electroretinogram (ERG) and EEG, they reported period doubling regime in response to stimuli between 30 Hz and 70 Hz [12].

Herrmann conducted an extensive study in which he used a square wave light source as the flickering stimulus to induce SSVEP responses in EEG [6]. He varied the stimulus frequency from 1 Hz to 100 Hz with 1Hz steps and reported that subharmonic oscillations occur near alpha band. He did not state any specific range of stimulation frequencies that yields period doubling behavior. From the data and graphs presented in his paper, it is observed that period doubling occurs in response to roughly half of the stimulation frequencies in the range of 15-30

Hz.

Tsoneva et al. have used repetitive visual stimuli in 40-60Hz (gamma band) to study temporal and spatial properties of SSVEP and analyze the interaction between SSVEP and ongoing brain rhythms. They have used square wave light source with 2Hz steps, excluding 50Hz. They reported subharmonic responses throughout this stimulus frequency range along with valuable spatiotemporal information regarding SSVEPs [13].

Roberts and Robinson used Robinson's Thalamocortical Model [74, 63, 75] to simulate Herrmann's experimental procedure and the model predicted similar results [15] to Herrmann's experimental results. They reported period doubling behavior for stimulus frequencies 15-24 Hz. They have also pointed out that square wave contains harmonic components by itself and is not the best stimulus for obtaining the most accurate results. So, they proceeded to apply sinusoidal flicker instead of square wave flicker to the model and came up with similar predictions [15]. They also stated that these predictions regarding sinusoidal excitation should be experimentally verified.

Labecki et al. undertook both experimental and simulation studies. They conducted an SSVEP experiment in which they used both square wave and sinusoidal light sources as the flickering stimuli to induce SSVEP responses in EEG [14]. Their experiment was rather limited in scope; they used 2 distinct frequency values for both modulation types (namely 5 Hz and 15 Hz). They stated that in the spectrum of EEG response to 15 Hz stimulus frequency, 7.5 Hz peak was statistically significant; however it is not clearly observable by the eye. They also applied their experimental procedure to Lopes da Silva's simple cortex model [76] to reproduce their experimental findings [14]. They reported that subharmonic responses occur in response to stimulus frequency range of 17-21.5 Hz when the input was square wave and 15-22 Hz when the input was sinusoidal wave.

In this part of the study, we took an experimental approach with the aim of (i) piecing together the earlier experimental results and (ii) statistically exploring the consistency of period doubling behavior for a subject and across subjects.

3.2 Methodology

3.2.1 Experimental Procedure

A total of 9 healthy (no neurological or psychiatric disorders) subjects with a mean age of 22 (6 males, 3 females) participated in the experiments. All subjects have normal or corrected-to-normal vision. All subjects signed an informed consent form which explains the objectives of the study and that flicker stimulation may cause epileptic seizures.

A simple Do-It-Yourself (DIY) cardboard VR headset with two, white, high gloss, 5 mm light-emitting diodes (LEDs) inside, where these two LEDs stay 2-3 cm in front of subjects' eyes, was built for the purpose of full visual field illumination 3.1. The stimulus is modulated with a sinusoidal waveform at 100% modulation depth. The peak illuminance at 2cm away from one of the LEDs is 410 lux as measured by Trotec BF06 luxmeter.

Figure 3.1: A photo of Do-It-Yourself (DIY) card-board VR headset

An FPGA board (Nexys 2^{TM} Spartan-3E FPGA Trainer Board (Digilent Inc, United States) with a 50 MHz crystal oscillator (100ppm tolerance)) is used to generate a very accurate sinusoidal waveform (with less than 1mHz error). This digital sinusoidal waveform was converted to a sinusoidal voltage waveform by a 12-bit D/A converter (MCP4921-E/P). To convert the voltage waveform

generated by the FPGA to light modulation, the circuit in Figure 3.2 is used. The input to this circuit has $3.3V$ peak-to-peak sinusoidal wave with $1.65V$ DC offset voltage. The max. current in this configuration is $3.3V/1.2k\Omega = 2.75mA$. This circuit is linear as long as the transistor is used in its non-sat region. The LEDs are driven at their linear region.

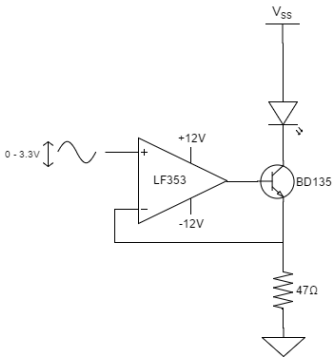

Figure 3.2: Stimulus circuit is used to convert voltage waveform to light waveform

To make sure that the generated sinusoidal light waveform is free of harmonics and is a "pure" sinusoid, the measurement circuit in Figure 3 is used. This circuit utilizes a PIN photodiode (BPW24), whose response is very linear when reverse biased [77], to convert the light intensity into voltage waveform. The reverse current through the diode generates a voltage at the OPAMP output. The generated light had a 40 dB difference between the first and second harmonic.

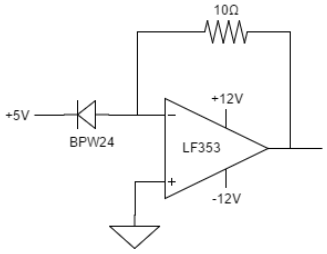

Figure 3.3: PIN Diode circuit is used to measure the light waveform generated by the circuit in Figure 3.2

Seven out of nine subjects participated in two different sets of experiments.

They were first presented a frequency range of 15 Hz to 32 Hz with 1Hz steps (experiment E1). On another day (within 2 weeks), they were presented a frequency range of 28 Hz to 42 Hz with 1Hz steps (experiment E2). We divided the stimulation frequencies into two experiments in order not to exhaust the participants and also to observe long-term differences regarding period doubling generation. Additionally, to test the short-term repeatability of our experimental procedure and also to observe the short-term variability of our findings, five out of nine subjects participated in 5 experiments in a row, in which they were presented a frequency range of 25 Hz to 35 Hz with 1Hz steps, keeping the same cap and electrodes in position. There was a 10-minute rest period between each successive experiment.

For all experiments, at each frequency, sinusoidal light was presented for 30 seconds with 10 seconds rest in between during which constant light at a level of half of the maximum brightness (LED circuit is driven by the DC offset voltage) was applied. An experiment was over when all the frequencies were presented once to the subject. For example, for 15-32 Hz experiment, there were 18 30-second recordings during which the stimulus was presented. In the beginning of each period of the sine wave, a marker pulse was also transmitted from FPGA to the EEG amplifier. For instance, for a 30 Hz sine wave, 900 markers were sent to the EEG amplifier during the 30 second stimulus presentation.

3.2.2 Data Acquisition

EEG was recorded with Brain Products V-Amp 16 channel EEG amplifier along with actiCAP, a standard 10-20 EEG cap with 32 electrode sites (Brain Products, Gilching, Germany). EEG was recorded from electrodes "O1, Oz, O2, Pz, P3, P4" and they were referenced to FCz electrode. The ground electrode was placed over nasion, on the forehead. BrainVision Recorder was used to record the EEG and marker pulses simultaneously. The electrodes are active and ImpBox (Brain Products, Gilching, Germany) was used to measure the impedance values of electrodes. Electrode impedances were kept below $10k\Omega$. The sampling rate

was $1kHz$. Data were filtered with a 50Hz Notch filter during recording.

3.2.3 Data Analysis

The EEG recordings were first exported to MATLAB using BrainVision Analyzer software and were analyzed in MATLAB (The MathWorks, Inc., Natick, MA, USA). For each experiment, 5–100 Hz bandpass filter was applied to each 30-second recording since fundamental frequency, its harmonics and subharmonics lie within this range and also to eliminate DC offset and slow components due to head movements. For each channel, from the 30-second recording of each frequency stimulation, fifteen non-overlapping 2-second long epochs were extracted. Epochs are chosen to be 2-second long to ensure that the subharmonic frequencies of odd stimulus frequencies have an integer number of cycles in an epoch. SSVEPs are typically observed from frequency spectrums of EEG recordings. For each stimulation frequency and for each channel, three different types of power spectrum density (PSD) estimates were calculated:
(i) PSD estimate of the 30-second long data,
(ii) average of PSD estimates of each epoch,
(iii) and PSD estimate of the average of fifteen epochs.

For PSD estimate calculations, Welch's method was used. In addition to the standard PSD plots, a two dimensional plot was also generated for the spectrums of the averaged epochs. In this plot, the stimulation frequencies are placed on the horizontal axis and the PSD estimate of the response to each stimulus frequency are gray-scale coded on the vertical axis (such as in Figures 3.6 and 3.7). This plot is called PSD versus Stimulus Frequency (PSD-SF) plot in the rest of this document for easy referral.

To determine if a subharmonic component (corresponding to period doubling) occurs or not, the PSD of half frequency component should be clearly distinguishable in amplitude (an outlier) from surrounding frequency components. The PSD estimate of 30-second long data was calculated with a frequency resolution of 0.1

Hz. From this data, a 21-point array that holds the PSD estimates in the [subharmonic frequency ± 1Hz] interval was extracted. For example, if the stimulation frequency was 30Hz, this array would be composed of PSD estimates of 14Hz to 16Hz with 0.1 Hz steps. To detect the occurrences of period doublings, MATLAB's "isoutlier" function was used on the extracted array. Outliers, which were more than three times the scaled median absolute deviation (MAD) away from the median, were detected from this array. If the detected outlier was found to be at the half fundamental frequency, then this outlier was regarded as a subharmonic occurrence and subharmonic occurrence value was assigned the value of '1' (else as '0'). For all experiments, subharmonic occurrences were identified by using the above method for each stimulus frequency in all channels.

Subharmonic Occurrence Rate across channels (SORc) for any given frequency and experiment was defined as average occurrence in all the six channels that were recorded. For the case of short term repeatability experiments, in addition to SORc values, Subharmonic Occurrence Rate across experiments (SORe) for any given frequency and channel was defined as average occurrence in all the 5 consecutive experiments. ANOVA was done on the SORc and SORe values of short term repeatability experiments to obtain statistical results. For both ANOVA tests, the independent variable was the stimulation frequency and the dependent variable was SOR. We have chosen to base our statistical decisions on a significance level of $p = 0.05$.

3.3 Experimental Results

To illustrate the benefit of averaging in data analysis, spectrum of a raw epoch and the spectrum of the average of the fifteen epochs within a 30-second recording are compared in Figure 3.4. It can be seen that averaging highly attenuates the alpha power (8-12 Hz) which exists in the raw recording. This happens because alpha components are not synchronous with the applied stimulus frequency and therefore they diminish with averaging. In the spectrum of the averaged

epoch (Figure 3.4(d)), the fundamental (32Hz), harmonic (64Hz) and subharmonic (16Hz) peaks are more easily observable than in the spectrum of the raw epoch (Figure 3.4(b)).

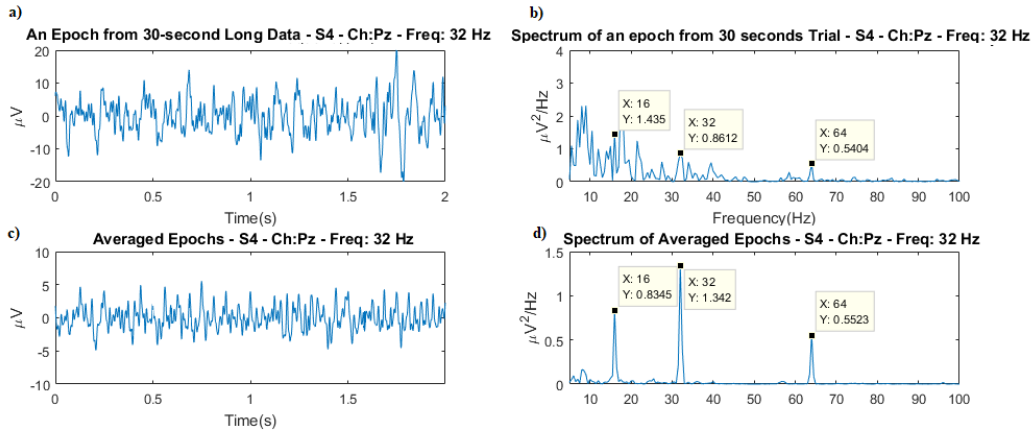

Figure 3.4: Effect of averaging on the PSD estimate. Data belongs to S4 (channel Pz, stimulus frequency = 32Hz). a) An example of an epoch (between 20th and 22nd seconds), and b) its spectrum. c) Average of the fifteen epochs of the 30-second recording, and d) its spectrum. The peaks on different spectrums are marked with data tips. Note that a) has 2 times the scale of c).

Figure 3.5 compares the three different PSD estimates that are explained in Data Analysis section. With a stimulation frequency of 40Hz, in the first type of PSD plot (Figure 3.5(a)), there is a clear high amplitude 20Hz signal component along with the expected 40Hz signal component. In the second type of PSD plot (Figure 3.5(c)), the subharmonic (20Hz) component is not as distinguishable from the surrounding spectral components. In the third type of PSD plot (Figure 3.5(d)), the 20Hz component is again more clearly evident. This figure again clearly demonstrates that signal averaging helps to suppress the alpha components and thereby enhances the appearance of the subharmonic component. Among the three types of spectrums presented in Figure 3.5, although subharmonic components are observable in all three, type 3 spectrums are especially preferable to obtain PSD-SF plots because with the other two types of spectrums, the stronger alpha range and nearby spectral components preclude the clear demonstration of period doubling on a PSD-SF plot.

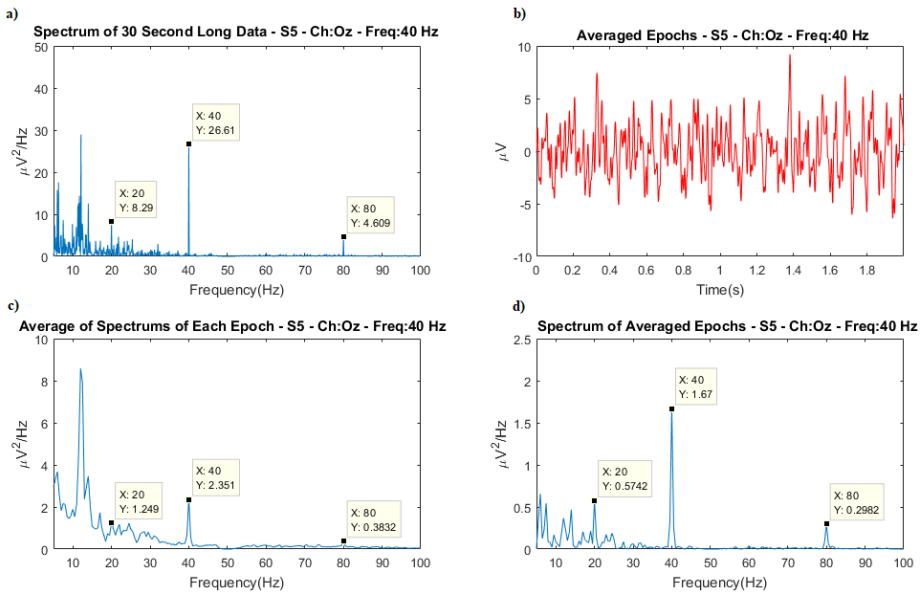

Figure 3.5: Comparison of the three types of PSD estimates. Data belongs to S5 (channel Oz, stimulus frequency = 40Hz). a) PSD estimate of 30-seconds long data b) Average of fifteen epochs. c) Average of PSD estimates of each epoch. d) PSD estimate of the average of fifteen epochs shown in b). The peaks on different spectrums are marked with data tips.

PSD-SF plot averaged across all subjects (for channel Oz) for experiment E1 (with 15-32 Hz stimulation range) is given in Figure 3.6. Components on the 1:1 line, on which the fundamental frequency components line up, are clearly visible. In a similar manner, the 2:1 line, on which the second harmonic components line up, is observable. The subharmonic components, which are to be on the 1:2 line, are also visible throughout this frequency range. Figure 3.7 presents the PSD-SF plot averaged across all subjects (for channel Oz) (data from subject S6 was discarded due to EEG artifacts for this recording) for experiment E2 (with 28-42 Hz stimulation range). As expected, the 1:1 and 2:1 lines (fundamental and second harmonics) are clearly visible. As the excitation frequency (stimulus) is increased from 28 to 42 Hz, a distinct and significant half frequency component follows (1:2 line). Subharmonic responses are more clearly discernable in Figure 3.7 than in Figure 3.6 because the subharmonic frequencies in Figure 3.7 do not fall in the alpha band. Subharmonic responses in Figure 3.6 are still visible within the alpha

band due to the existence of a frequency dependent trend. If signal averaging is not used before PSD estimation, this trend is not visible.

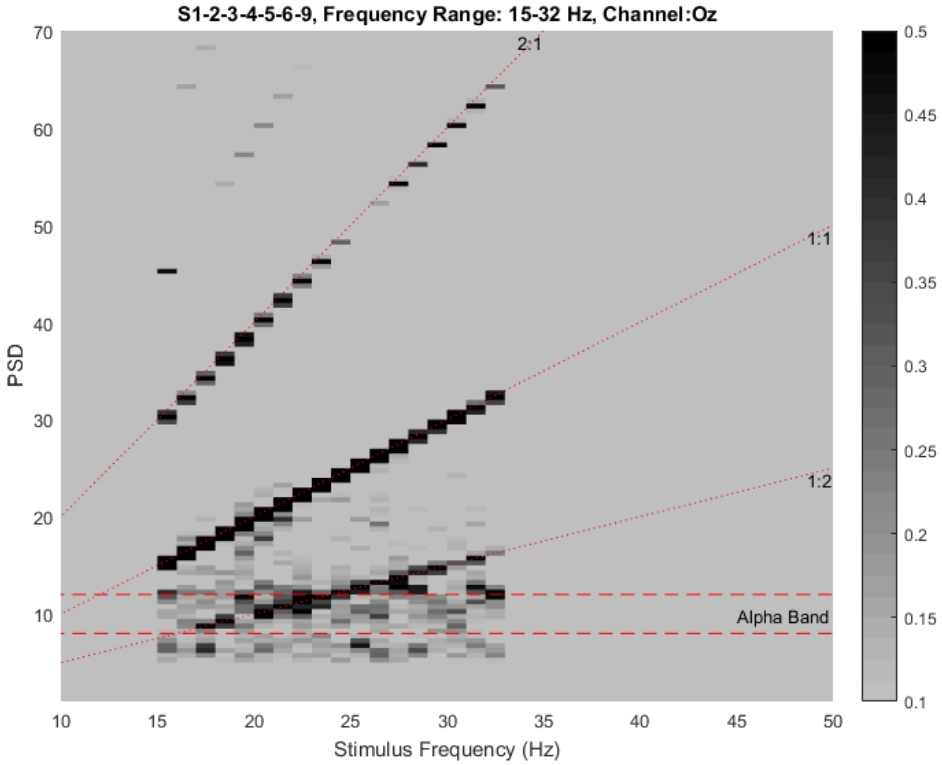

Figure 3.6: Averaged PSD-SF plot across all subjects (Channel Oz) for the experiment that covers the stimulus frequencies from 15Hz to 32Hz. Horizontal dashed red lines visualize the alpha band (8-12 Hz interval). The dotted red lines are put for better demonstration of the trends in data. The lower limit of the colorbar is set to 0.1 to eliminate confusion due to background noise in spectrums. The upper limit is saturated at 0.5 for clear observation of subharmonic peaks.

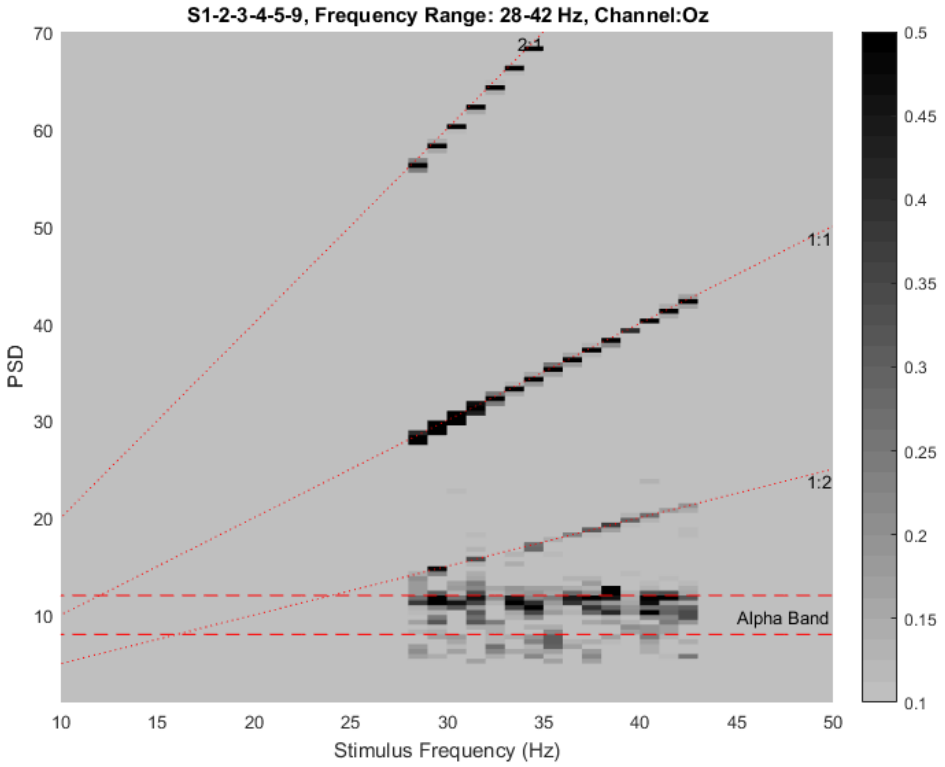

Figure 3.7: Averaged PSD-SF plot across all subjects (Channel Oz) (data from subject S6 was discarded due to EEG artifacts for this recording) for the experiment that covers the stimulus frequencies from 28Hz to 42Hz. Horizontal dashed red lines visualize the alpha band (8-12 Hz interval). The dotted red lines are put for better demonstration of the trends in data. The lower limit of the colorbar is set to 0.1 to eliminate confusion due to background noise in spectrums. The upper limit is saturated at 0.5 for clear observation of subharmonic peaks

Table 3.1 presents at which frequencies period doubling is observed for each subject in the 15-32 Hz and 28-42 Hz experiments. Considering the 15-32 Hz experiments (E1), in three subjects (subjects S1, S5 and S9), period doubling is observed throughout nearly the whole frequency range (for subjects S1 and S9, the observed frequencies are contiguous and for subject S5 the frequencies that depict period doubling are separate (spaced)). For subjects S2, S3 and S6, period doubling is observed in the second half of the stimulus frequency range

(from 25 Hz and onward). For subject S4 on the other hand, period doubling is not observed at all. In the 28-42 Hz experiments (E2), out of the 15 stimulation frequencies, subjects S2, S9, S3, S5, S1, S4 and S6 generate subharmonic responses at 10, 10, 9, 8, 7, 5 and 5 frequencies respectively. S2, S3, S4 and S9 depict contiguous responses but the others have spaced-out responses. Therefore, there is substantial subject to subject variation regarding the frequencies of period doubling phenomena. Furthermore, for a given subject, considering the overlapping stimulation frequencies in both experiments (28-32Hz), experiments performed in different days also may yield different results.

Table 3.1: Stimulus frequencies for which period doubling is observed in two different experiments (E1: Stimulus frequencies 15-32 Hz and E2: Stimulus frequencies 28-42 Hz) for seven subjects. Green highlight is used when period doubling behaviour is present and red highlight is used when not. The presence of period doubling is determined according to SORc for each frequency (Present if SORc $> 50\%$). First column lists the subject IDs. Second column lists the stimulus frequencies for which period doubling is observed for E1. Third column lists the stimulus frequencies for which period doubling is observed for E2.

Subject No	**15-32 Hz Experiment (E1)**	**28-42 Hz Experiment (E2)**
S1	16, 17, 18, 19, 20, 22, 23, 24, 25, 26, 27, 28, 29, 31 Hz	28, 29, 30, 31, 38, 41, 42 Hz
S2	27, 28, 29, 30, 31, 32 Hz	29, 30, 31, 32, 33, 34, 35, 36, 37, 39 Hz
S3	30, 31, 32 Hz	34, 35, 36, 37, 38, 39, 40, 41, 42 Hz
S4	Not Present.	28, 29, 30, 31, 32 Hz
S5	17, 20, 24, 25, 28, 31 Hz	30, 32, 36, 37, 38, 40, 41, 42 Hz
S6	25, 26, 28, 30 Hz	30, 33, 34, 37, 41 Hz
S9	17, 18, 19, 20, 22, 23, 24, 29, 30, 31 Hz	28, 29, 30, 32, 34, 36, 37, 38, 39, 40 Hz

Table 3.2 shows the Subharmonic Occurrence Rates across channels (SORc) for subject S3 within the 5 consecutive experiments which were performed for observing the short term repeatability of the experimental procedure. From Table 3.2, SORc value, averaged across all frequencies (bottommost row) for a single experiment is observed to vary from a minimum of 24% to a maximum of 52%. The change in this rate does not follow a trend in time (experiment number). One-way repeated measures ANOVA test [78] (which is an extension of the paired t-test) concludes that, when all frequencies are considered together, the experiments do not differ significantly ($F(4,40) = 1.322$, $p = 0.2783$). Similar results are obtained for the other subjects except for subject S2 (see Table 3.4 for statistical details). In S2 experiments are found to be different and however, this is only due to the difference between experiment 1 and experiment 4 revealed by a post-hoc test which analyzes experiments in pairs ($p=0.035$). On the other hand, even between experiments which are not found to be different statistically when all frequencies are considered together, there are substantial individual variations in SORc values when a single frequency is considered. For example, for 31Hz SORc value varies from 100% to 0% across experiments in Table 3.2.

Table 3.2: SORc values of each stimulation frequency in 5 consecutive repeatability experiments for S3. First column lists the stimulation frequencies used in all 5 experiments. Second to sixth columns list the corresponding SORc values in different experiments.

Stimulus Frequency	**Exp1**	**Exp2**	**Exp3**	**Exp4**	**Exp5**
25Hz	0%	83%	67%	17%	17%
26Hz	83%	0%	33%	0%	33%
27Hz	0%	50%	50%	50%	67%
28Hz	67%	67%	83%	50%	17%
29Hz	67%	17%	17%	0%	33%
30Hz	83%	83%	83%	17%	67%
31Hz	100%	83%	33%	0%	33%
32Hz	50%	0%	17%	67%	0%
33Hz	83%	83%	17%	17%	33%
34Hz	33%	0%	50%	33%	0%
35Hz	0%	50%	50%	17%	100%
Avg.	52%	47%	45%	24%	36%

For a reason explained later in the Conclusions and Discussion section, we have also investigated if there is significant difference between occipital channels (O1,Oz,O2) and parietal channels (P3,Pz,P4). Table 3.3 shows the average of Subharmonic Occurrence Rates across experiments (SORe) of O channels and P channels for subject S3. One-way ANOVA test shows that there is no significant difference between O channels and P channels ($F(1,20) = 2.61$, $p = 0.122$) for S3. In fact, as shown in the second column of Table 3.4, one-way ANOVA concludes that O channels and P channels do not differ significantly in all subjects (F and p values are given in Table 3.4).

Table 3.3: Average SORe values for each stimulation frequency in O and P channels for S3. First column lists the stimulation frequencies used in all 5 experiments. Second column lists the average of the SORe values of O1,Oz,O2 channels. Third column lists the average of the SORe values of P3,Pz,P4 channels

Stimulus Frequency	**Oavg**	**Pavg**
25Hz	40%	33%
26Hz	33%	27%
27Hz	53%	33%
28Hz	60%	53%
29Hz	33%	20%
30Hz	67%	67%
31Hz	53%	47%
32Hz	27%	27%
33Hz	47%	47%
34Hz	33%	13%
35Hz	60%	27%
Avg.	46%	36%

The SORc and SORe values for the other subjects (S2, S4, S7, S8) are given in the Appendix as tables with same structure as Tables 3.2 and 3.3.

Table 3.4: Summary of obtained results for the 5 consecutive repeatability experiments that are done on five subjects for observing the short term repeatability of the experimental procedure. First column lists the subject IDs. Second column lists the statistical results (F and p values) of one-way repeated measures ANOVA for each subject to test the short term repeatability. Third column lists the statistical results (F and p values) of one-way ANOVA for each subject to compare the subharmonic occurrence in O and P channels

Subject No	**Statistical Results Between Experiments**	**Statistical Results Between Channels**
S2	Differ significantly, $F(4,40) = 3.573$, $p = 0.0139$	Do not differ significantly, $F(1,20) = 0.11$, $p = 0.7528$
S3	Do not differ significantly, $F(4,40) = 1.322$, $p = 0.2783$	Do not differ significantly, $F(1,20) = 2.61$, $p = 0.122$
S4	Do not differ significantly, $F(4,40) = 1.506$, $p = 0.2187$	Do not differ significantly, $F(1,20) = 0.063$, $p = 0.8063$
S7	Do not differ significantly, $F(4,40) = 0.70$, $p = 0.5968$	Do not differ significantly, $F(1,20) = 0.40$, $p = 0.5335$
S8	Do not differ significantly, $F(4,40) = 1.73$, $p = 0.1615$	Do not differ significantly, $F(1,20) = 0.08$, $p = 0.7848$

We have also studied the variations of the subharmonic peak relative to the fundamental peak. Indeed, as shown in Figure 3.8 as an example, the ratio of the amplitude at the subharmonic frequency to the fundamental component is less than one in 27-30 Hz region and larger than one at 31Hz and 32Hz for subject S2 (Channel Oz). In general, considering the observations in all experiments of the study, the amplitude of the subharmonic frequency relative to the amplitude of the fundamental frequency does not follow a trend and is variable with respect

to frequency. Figure 3.9 shows the change in relative amplitude for subject S2's repeatability experiments. In this figure, it can be observed that relative amplitudes vary with respect to frequency for an experiment and vary with respect to experiment for a frequency. It can also be seen that although relative amplitude generally resides below 1, there are cases when subharmonic component is much larger than the fundamental component.

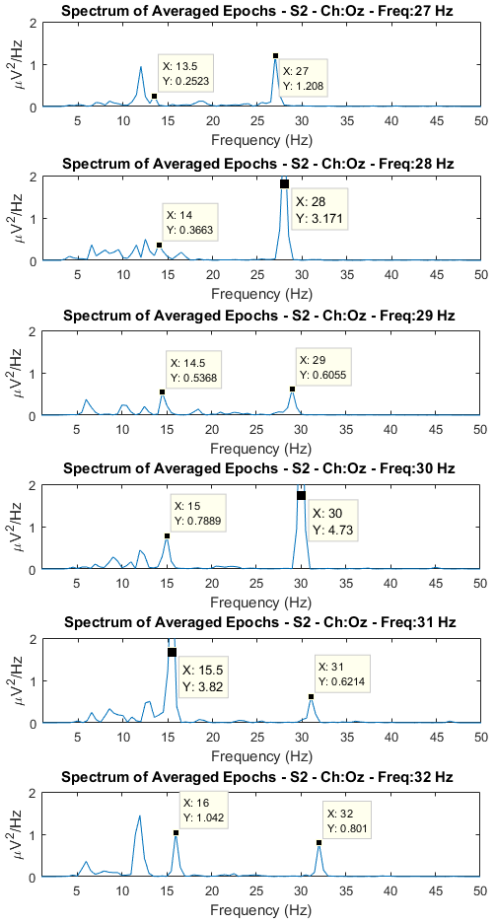

Figure 3.8: The power spectrums of averaged epochs for 27Hz to 32Hz stimulus frequencies. Data belongs to S2 (Channel Oz). The peaks on different spectrums are marked with data tips. The ratio of the amplitude at the subharmonic frequency to the fundamental component is varying. Note that some peaks are outside the vertical range, their peak values can be seen on the corresponding data tip.

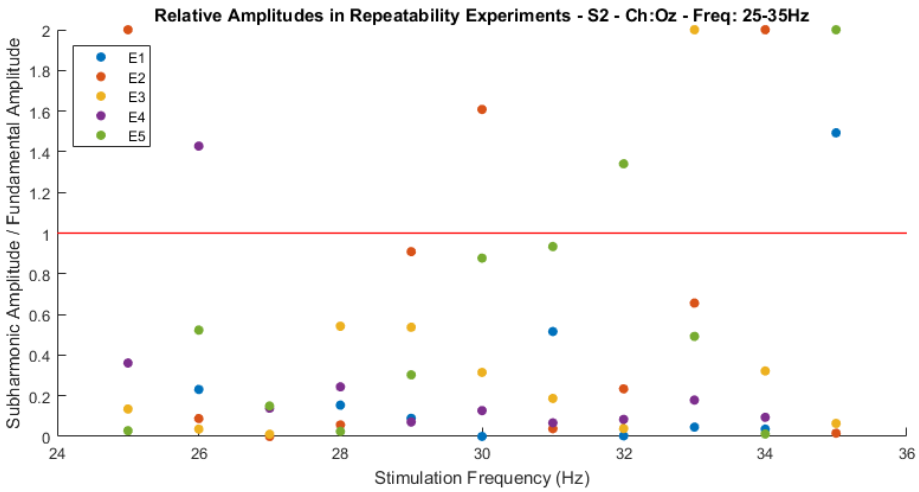

Figure 3.9: Ratio of amplitudes of subharmonic responses to the amplitudes of fundamental responses in five consecutive repeatability experiments of subject S2 (Channel Oz). Relative amplitude is varying in the short term for each frequency. Experiments 1 to 5 are colour coded. Notice that ratios greater than 2 are saturated at 2 for better demonstration. The horizontal red line corresponds to the ratio of 1.

3.4 Discussion of Experimental Results

Our experimental results indicate that period doubling may occur in all stimulation frequencies (15-42 Hz) that our experiments have covered. In earlier studies, which covered a broad range of stimulation frequencies (1-100 Hz), Herrmann's findings indicated subharmonic generation for the stimulus range of 15-30 Hz [6], and Crevier and Meister reported subharmonic occurrence range for stimulus frequencies between 30-70 Hz [12]. Additionally, Tsoneva et al. have studied the stimulus frequency range of 40-60 Hz and have observed subharmonic generation in this frequency range [13]. Therefore, considering the results of all these studies and the current study, it is likely that subharmonic generation occurs in a broad range of frequencies, and for the present moment, an exact frequency range of subharmonic generation cannot be stated. The differences between the results of

different studies may perhaps be explained by factors specific to the subjects included in the experiments and also specific to the experimental conditions, which however need to be identified in further studies.

The mechanisms of subharmonic frequency generation is still an unresolved issue. In the 2012 study of Roberts and Robinson [15], Robinson's Thalamocortical model [74, 63, 75] was tuned to reproduce Herrmann's findings [6] and, the model showed period doubling behaviour only in 15-24 Hz stimulus interval. Similarly, Labecki et al. [14] used Lopes da Silva's cortical column model [76] to reproduce period doubling behaviour in 15-22 Hz stimulus interval. However, our study indicates that a model should include a broader frequency region in its period doubling regime. Future models should be able to provide means for the tuning of subharmonic frequency range and preferably be able to relate these to physiological and environmental conditions (such as those mentioned in the next paragraph). It is vital to adjust these models according to such factual experimental information so that model predictions, regarding other nonlinear phenomena and dynamics and physiological mechanisms, could be basis for further research.

The summarized results in Table 3.1 suggest that there is substantial inter-subject variability and also substantial intra-subject variability among experiments that are conducted in different days. We have also conducted on five subjects the so called short-term repeatability experiments in order to observe the short term effects on subharmonic generation. Although, period doubling generation is mostly consistently observed in consecutive experiments when all frequencies are considered together, there is considerable variation in the SOR values of a frequency across experiments. It may be conjectured that both long term effects (electrode placement, physiological state, psychological state, illness, hunger, etc.) and short term effects (changes in gaze, attention level, fatigue etc.) may be factors that cause these variations.

The effect of attention on SSVEP fundamental peak amplitude is investigated in [79]. Mutual influence between fatigue level and SSVEP parameters have also been reported in [80]. Level of attention and fatigue may also be altering period doubling generation. In any case, it may be wise to conduct SSVEP

experiments, which aim at investigating subharmonic frequency generation, with random stimulus frequency order to eliminate the doubt related to fatigue and attention. Random stimulus frequency order may also be important to circumvent possible biases due to hysteresis effects predicted by Roberts and Robinson in their simulation study [15].

From the ERG recordings of both humans and animals, period doubling behavior was reported [12, 81, 82] which indicates that subharmonic generation can occur at the retina. Lateral geniculate nucleus (LGN) takes inputs from retinal ganglion cells and projects most of its output to primary visual cortex which are then projected to other visual cortex areas [83]. The electrode sites, O1, Oz and O2 that were used in our experiments, correspond to primary (Oz) and secondary visual (O1, O2) cortices [84]. Accordingly, in our repeatability experiments, we argued that subharmonic occurrence rates may be consistently different between O and P channels. However, the statistical analysis we have performed on the repeatability experiments yielded no difference between channels (See Table 3.4).

As shown in Figure 3.9, the ratio of subharmonic to fundamental component amplitudes varies considerably. In fact, there are cases where a fundamental peak may not occur at all while a subharmonic component occurs (such cases are saturated with a ratio of 2 in Figure 3.9). The amplitudes of subharmonic and fundamental components also change considerably from channel to channel. There may even be some extreme cases such as shown in Figure 3.10(a) and Figure 3.10(b) where fundamental component is almost non-existent in channel O1 whereas it is of the same order of magnitude with subharmonic component in channel Oz. Figure 3.10(c) shows an example of another nonlinear interaction that is not as commonly visible as other observed nonlinear phenomena. There is a peak at third harmonic of the subharmonic frequency ($f + f/2$, where f is the stimulation frequency) in SSVEP spectrum. It is not clear whether such behavior is a result of nonlinear interactions of different cortical areas or maybe an inherent property of the cortex in general.

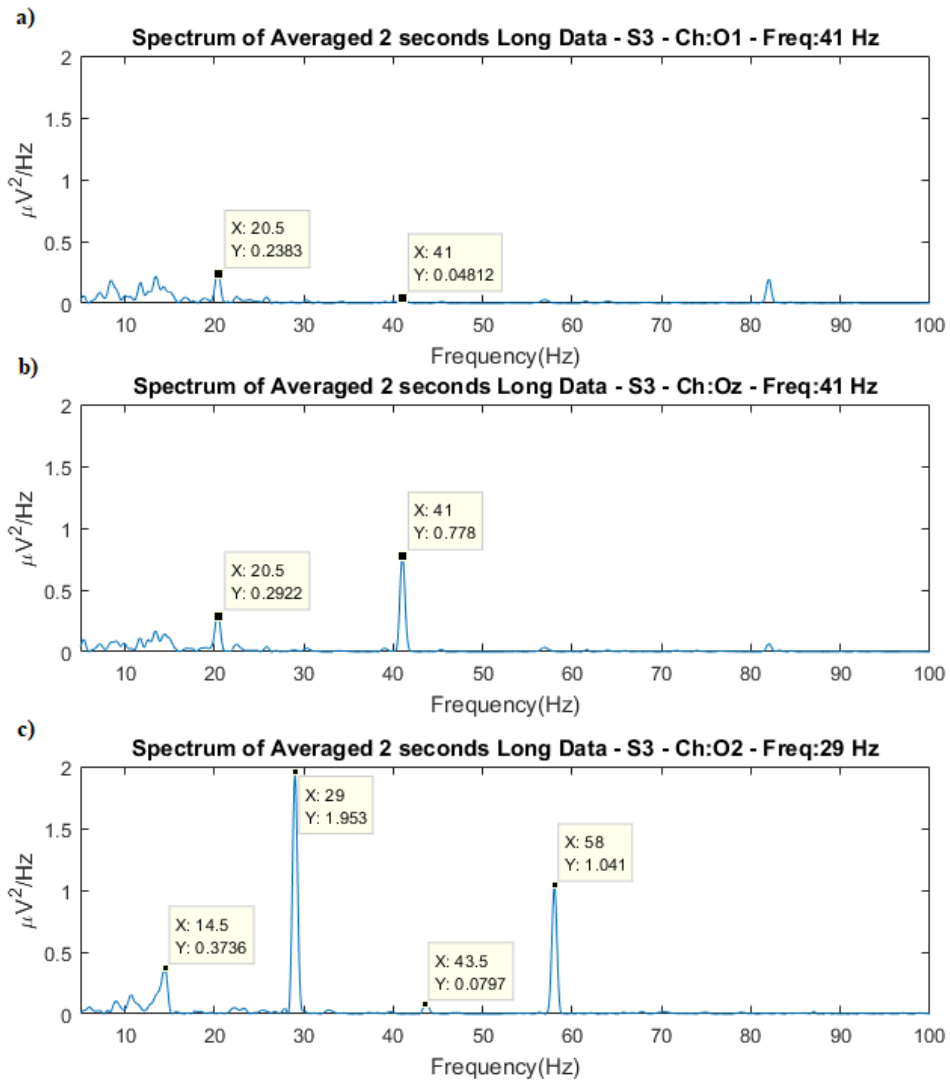

Figure 3.10: Other observed nonlinear characteristics of SSVEP response. Data belongs to S3. a) Spectrum of averaged epochs in channel O1. Fundamental frequency (stimulus frequency) is 41Hz. b) Spectrum of averaged epochs in channel Oz. Fundamental frequency (stimulus frequency) is 41Hz. c) Spectrum of averaged epochs in channel Oz. Fundamental frequency is 29Hz (denoted by f). Strong subharmonic (f/2) and harmonic (2f) peaks are present in the spectrum. An additional peak at 43.5Hz (f+f/2 = 3f/2) is visible for this particular case. This phenomenon is actually present in many recordings, but is not always as obvious as in this case.

SSVEP is widely used in BCI applications due to its robustness and speed [5, 85, 86]. The reported phenomena in the current study includes cases in which subharmonic peaks are greater in amplitude than fundamental peaks or in which fundamental peaks are non-existent while subharmonic peaks are clearly observable. In a BCI application using the SSVEP paradigm, total lack of fundamental component would likely degrade classification accuracy. Thus, it can be claimed that utilizing subharmonic peaks in addition to fundamental peaks in SSVEP responses would improve BCI performance. This requires target frequencies to be chosen for a particular subject within the frequency range where period doubling behaviour is observed. Similarly, since the second harmonic components are consistently observed in all of our experiments, additional use of this harmonic in SSVEP BCI applications is also justified.

Chapter 4

Model Based Investigation of Period Doubling Behavior in Human SSVEP Responses

4.1 Earlier Modeling Studies Regarding SSVEPs

Modeling studies usually focus on the linear responses and properties of the model under no drive (or when driven by noise). These are generally brain rhythms and stability boundaries of the system. More recently, driven brain activity seems to attract increasing interest, bringing nonlinear interactions to investigators' attention. Spiegler et al. [16] have investigated the photic driving effect (i.e. frequency entrainment) of a periodic light stimulus through a modified Zetterberg-Jansen model [87]. They drove the model with a rhythmic input consisting of a train of pulses where each pulse is similar to that used by Jansen and Rit [87]. Then, they demonstrated many different nonlinear dynamics the model can produce, including chaos. Particularly, they investigated the effect of stimulus amplitude on the entrainment phenomenon and came up with various predictions. In this work, however, authors did not mention any subharmonics generated by the cortical model.

Roberts and Robinson have driven Robinson's Corticothalamic Model [74, 63, 75] with periodic input (square and sine wave). They tested the model against Herrmann's experimental findings [6] and came up with very accurate predictions. Their observations included subharmonic components at the model output for stimulus frequencies between 15-24 Hz but they did not discuss the possible mechanisms of generation of such components. They rather focused on entrainment of the alpha rhythm to the fundamental as well as the subharmonic components.

Labecki et al. have driven the neural mass model by Lopes da Silva et al. [76] with periodic input (square and sine wave) [14]. They observed subharmonic responses in the model output for stimulus frequencies (for sine wave input) between 17-21.5 Hz. They also claimed that for subharmonic oscillations to occur, a feedback loop with at least one nonlinear element is necessary in the mathematical sense.

In this part, we have employed a modeling approach and compared its predictions with experimental results detailed in the previous chapter and also in [88]. We have also identified other important aspects of the subharmonic generation in the model.

4.2 Methodology

4.2.1 Model Implementation

In this work, we use a neural field model that had been proposed by Robinson et al. to model cortico-thalamic dynamics [74, 63, 75]. This model includes three main neuronal populations, cortical neurons (excitatory (e) and inhibitory (i) interneurons and implicitly pyramidal cells), thalamic reticular (r) neurons and thalamic relay (s) neurons. In our experiments [88], we have used a full visual field stimulus (the DIY VR headset). This allows us to assume spatially uniform stimulation of the visual cortex, hence allowing us to model the entire

visual cortex with a single neuronal population. With such assumption, we also omit the spatial dependence of the model and thus reduce it to a neural mass model. Below we provide an explanation of the model formulations keeping the notation in the original work mostly unchanged [74, 63, 75].

In this model, each population is modeled by two main relations: (i) a linear operator $D_{ab} = \frac{1}{\alpha_{ab}\beta_{ab}}\frac{d^2}{dt^2} + (\frac{1}{\alpha_{ab}} + \frac{1}{\beta_{ab}})\frac{d}{dt} + 1$ that relates the mean postsynaptic potential V_{ab} of population a to the mean afferent firing rate ϕ_b coming from the presynaptic population b by $D_{ab}V_{ab}(\mathbf{r}, t) = v_{ab}\phi_b(\mathbf{r}, t - \tau_{ab})$. Here v_{ab} denotes the synaptic connection strength between populations a and b, τ_{ab} denotes the mean axonal delay between populations a and b, and β_{ab}, α_{ab} denote the reciprocal rise and fall times of the membrane potential of population a due to input coming from population b, (ii) a nonlinear shifted sigmoidal function $Q_a = S[V_a] = \frac{Q_{max}}{1+\exp(-(Va-\theta)/\sigma)}$ that relates the mean firing rate Q_a of population a to the same population's mean membrane potential $V_a = \sum_b V_{ab}$. Here, Q_{max} denotes the maximum firing rate, θ is the mean threshold voltage for the population and σ denotes the variance of this threshold value in the population.

Originally, the model regarded mean afferent firing rates ϕ_a as fields and these were governed by a damped wave equation with $Q_a = S[V_a]$ as the source:

$$[\frac{1}{\gamma_a^2}\frac{\partial^2}{\partial t^2} + \frac{2}{\gamma_a}\frac{\partial}{\partial t} + 1 - r_a^2\nabla^2]\phi_a((\mathbf{r}, t) = S[V_a(\mathbf{r}, t)] \tag{4.1}$$

where γ_a is the reciprocal delay due to axonal conduction and r_a is the axon length. However, in reducing the model to a neural mass model, we omitted the ∇^2 terms (since we assume there is no positional dependence in the cortex we also drop the $\mathbf{r}$ argument) for all populations $a = e, i, r, s$. For populations other than $a = e$ (i.e. for inhibitory interneurons and thalamic populations), axonal conduction delay $1/\gamma_a$ is taken to be zero, yielding

$$\phi_a(t) = S[V_a(t)] \tag{4.2}$$

for $a = i, r, s$ and

$$[\frac{1}{\gamma_a^2}\frac{d^2}{dt^2} + \frac{2}{\gamma_a}\frac{d}{dt} + 1]\phi_a(t) = S[V_a(t)] \tag{4.3}$$

for $a = e$.

Note that the operator in 4.3 is different from the two main relations explained above. Specifically, this does not convert firing rate to potential or vice versa, it is only introducing a delay to the excitatory population dynamics due to longer ranged axonal connections of the excitatory neurons.

The authors made further assumptions regarding intrathalamic and intracortical connectivities [15]: they took all $\beta_{ab} = \beta, \alpha_{ab} = \alpha$ (hence $D_{ab} = D_\alpha$) except for the intrathalamic β_{sr} and α_{sr} values (hence $D_{sr} \neq D_\alpha$) due to slower dynamics, and they took $V_e = V_i$ due to random intracortical connectivity.

Given above assumptions and derivations, the model equations are:

Contribution by firing rate coming from sensory population (ϕ_n) to mean membrane potential of thalamic relay population V_{sn}:

$$D_\alpha V_{sn}(t) = v_{sn}\phi_n(t) \tag{4.4}$$

Contribution by firing rate coming from thalamic reticular cell population (ϕ_r) to mean membrane potential of thalamic relay population V_{sr}:

$$D_{sr} V_{sr}(t) = v_{sr}\phi_r(t) \tag{4.5}$$

Contribution by firing rate coming from excitatory cortical interneurons (ϕ_e) to mean membrane potential of thalamic relay population V_{se}:

$$D_\alpha V_{se}(t) = v_{se}\phi_e(t - t_0/2) \tag{4.6}$$

Mean membrane potential of thalamic relay population V_s:

$$V_s(t) = V_{sn}(t) + V_{sr}(t) + V_{se}(t) \tag{4.7}$$

Contribution by firing rate coming from excitatory cortical interneurons (ϕ_e) to mean membrane potential of thalamic reticular population V_{re}:

$$D_\alpha V_{re}(t) = v_{re}\phi_e(t - t_0/2) \tag{4.8}$$

Contribution by firing rate coming from thalamic relay cell population (ϕ_s) to mean membrane potential of thalamic reticular population V_{rs}:

$$D_\alpha V_{rs}(t) = v_{rs}\phi_s(t) \tag{4.9}$$

Mean membrane potential of thalamic reticular population V_r:

$$V_r(t) = V_{re}(t) + V_{rs}(t) \tag{4.10}$$

Contribution by firing rate coming from excitatory cortical interneurons (ϕ_e) to mean membrane potential of excitatory cortical interneuron population V_{ee}:

$$D_\alpha V_{ee}(t) = v_{ee}\phi_e(t) \tag{4.11}$$

Contribution by firing rate coming from inhibitory cortical interneurons (ϕ_i) to mean membrane potential of excitatory cortical interneuron population V_{ei}:

$$D_\alpha V_{ei}(t) = v_{ei}\phi_i(t) \tag{4.12}$$

Contribution by firing rate coming from thalamic relay cell population (ϕ_s) to mean membrane potential of excitatory cortical interneuron population V_{es}:

$$D_\alpha V_{es}(t) = v_{es}\phi_s(t - t_0/2) \tag{4.13}$$

Mean membrane potential of excitatory cortical interneuron population V_e:

$$V_e(t) = V_{ee}(t) + V_{ei}(t) + V_{es}(t) \tag{4.14}$$

Mean afferent firing rate ϕ_s of the thalamic relay population with a mean membrane potential of V_s:

$$\phi_s = S[V_s(t)] \tag{4.15}$$

Mean afferent firing rate ϕ_r of the thalamic reticular population with a mean membrane potential of V_r:

$$\phi_r = S[V_r(t)] \tag{4.16}$$

Mean afferent firing rate ϕ_i of the inhibitory cortical interneuron population with a mean membrane potential of $V_i = V_e$:

$$\phi_i = S[V_i(t)] = S[V_e(t)] \tag{4.17}$$

Mean afferent firing rate ϕ_e of the excitatory cortical interneuron population with a mean membrane potential of V_e:

$$[\frac{1}{\gamma_e^2}\frac{d^2}{dt^2} + \frac{2}{\gamma_e}\frac{d}{dt} + 1]\phi_e(t) = S[V_e(t)] \tag{4.18}$$

These differential equations are implemented and solved in MATLAB (The MathWorks, Inc., Natick, MA, USA) and C (implementation in C greatly boosts simulation speed which is very crucial for parameter sweep studies) with a forward Euler integration scheme with $dt = 10^{-4}s$. For the sake of easier analysis and modification of the model equations, we also implemented the model in Simulink (The MathWorks, Inc., Natick, MA, USA) environment. For this purpose, differential operators D_α, D_{sr} and D_{γ_e} are converted to transfer functions of the form:

$$D_\alpha \rightarrow H_\alpha(s) = \frac{\alpha\beta}{s^2 + (\alpha + \beta)s + \alpha\beta} \tag{4.19}$$

$$D_{sr} \rightarrow H_{sr}(s) = \frac{\alpha_{sr}\beta_{sr}}{s^2 + (\alpha_{sr} + \beta_{sr})s + \alpha_{sr}\beta_{sr}} \tag{4.20}$$

$$D_{\gamma_e} \rightarrow H_{\gamma_e}(s) = \frac{\gamma_e^2}{s^2 + (2\gamma_e)s + \gamma_e^2} \tag{4.21}$$

Then, the model can be expressed as a block diagram as in Figure 4.1. Here, when the cortical circuit is examined, one can interpret that pyramidal cell population is in fact explicitly modeled and the interneuron populations are implicitly modeled through synaptic strengths v_{ei} and v_{ee}. That is to say, output of the pyramidal cell population $S[V_e(t)]$ is scaled by gains v_{ei} and v_{ee} and then converted to contributions to mean soma potential of the pyramidal cell population (V_{ei} and V_{ee}). Hence we adopt V_e as the mean membrane potential of the pyramidal cell population which is thought to be the main source of recorded scalp EEG [89]. For the sake of consistency, Simulink is set to solve the model with a forward Euler integration scheme with $dt = 10^{-4}s$.

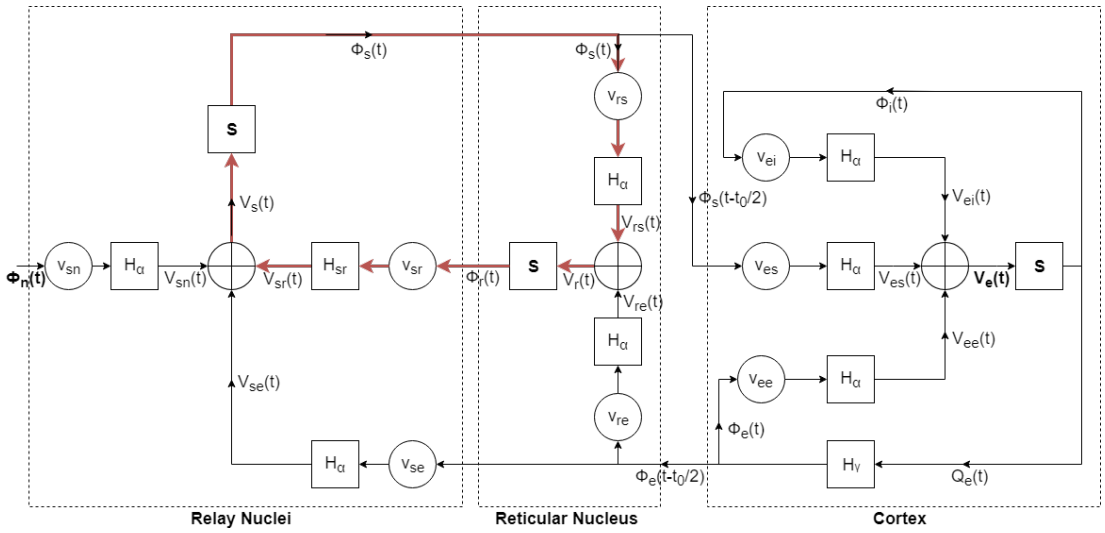

Figure 4.1: Representation of Robinson's Corticothalamic Model as a block diagram. There are three main populations in the model: (i) Relay Nuclei (ii) Reticular Nucleus (iii) Cortex. Their contents are marked with dashed boxes. There are three types of blocks in the whole model: (i) gain blocks denoted with v_{ab}, (ii) second order transfer functions denoted with H, (iii) sigmoidal type nonlinear blocks denoted with S. Input to the model is given via ϕ_n while the output is taken from V_e. Notice the red highlighted intrathalamic loop from which subharmonic oscillations seem to arise.

Since lateral geniculate nucleus of the thalamus acts as the relay station for sensory inputs coming to the brain [63] (hence the name relay nucleus in the model), input to the model (ϕ_n) is given via relay nucleus. We model the stimulus as background activity and stimulus superimposed:

$$\phi_n(t) = \phi_n^{BG} + \phi_n^{stim}$$

Here, ϕ_n^{BG} denotes the background activity. Generally, this activity is modeled as a Gaussian white noise. However, we believe the stimulus in our experiments would dominate the amount of noise in the background activity, so we only consider ϕ_n^{BG} as a constant value. ϕ_n^{stim} is simply a cosine at the stimulation frequency with amplitude Φ_n. In doing this, we make the assumption of ignoring the potential role of retinal dynamics in the experimentally observed PD phenomenon.

In earlier studies of this model, different values (or ranges) for different parameters were discussed [63, 90, 65]. These ranges were taken into consideration during parameter sweeps in the current study. In their 2012 study [15], Roberts and Robinson drove this model with a sinusoidal input and shared a parameter set that would better resemble the features and trends in the experimental data of Herrmann [6], however, they did not discuss about how they decided on the actual parameter values. In this work, we took their parameter set as the starting point and undertook our model analysis using these values. In the said analysis, we aimed to locate where in the model the subharmonic components originate from. To do so, we cut various feedback connections in the model and observed how the PD behavior in the output changed. We also supported this with rather limited (narrow scoped) parameter sweep studies. We refrained from doing an extensive parameter sweep study, because with such a high order model (i.e. 17 parameters) doing such a work requires substantial amount of computational power and time.

4.2.2 Describing Function

A conventional way of analyzing the nonlinear components in nonlinear feedback systems is via finding a describing function (DF) for the said nonlinear components. The DF in this context, relates the amplitudes and phases of the components in its output to those of the components in its input (i.e. it can be regarded as a relative amplitude and relative phase dependent transfer function). For polynomial type nonlinearities, describing functions can be analytically found [45, 44] but in our case the nonlinearity is a shifted sigmoid. Also, describing function analysis requires the linear part of the system to behave as a sharp low pass filter that filters out higher order components. However, for many values of the reciprocal time constants β and α (and others), this may not be the case in the model. These require DFs to be numerically computed by dividing the Fourier coefficients in its output to those in its input [44]. Calculating DFs for nonlinearities allows us to write loop equations and solve these for amplitudes and phases of the oscillations in the system output by utilizing a numerical nonlinear

system solver (such as fsolve in Matlab).

4.3 Model Analysis and Results

We first reproduced the results of Roberts and Robinson's study [15]. Here the parameters used are given in Table 4.1:

Table 4.1: The parameter set that we used to run the model and initially make our observations from. These values are taken from [15] where the authors drove this model with a sinusoidal input and shared a parameter set that would better resemble the features and trends in the experimental data of Herrmann [6].

$v_{se} = 2.9, v_{sr} = -0.57, v_{re} = 0.67, v_{rs} = 2.9, v_{sn} = 1, v_{ee} = 1.3, v_{ei} = -2.9, v_{es} = 0.13$
$\alpha = 80s^{-1}, \beta = 800s^{-1}, \alpha_{sr} = 10s^{-1}, \beta_{sr} = 60s^{-1}$
$Q_{max} = 250, \sigma = 3.3, \theta = 15$
$\phi_n^{BG} = 18, \phi_n^{stim} = 2.8$

A two dimensional plot, similar to what was used to visualize experimental results, was formed from the model responses to stimulation frequencies in the 1-50 Hz interval (Figure 4.2). It can be seen that alpha band power is concentrated at $f_\alpha = \ 11Hz$ (model's native oscillation frequency). Here it is obvious that, when driven with a sinusoidal input with an amplitude $\phi_n^{stim} = 2.8$ and bias $\phi_n^{BG} = 18$, the model can generate subharmonics in the $15 - 25Hz$ stimulus frequency region (and also f_α is entrained to the subharmonic frequency), but not at higher frequencies. It is of interest to investigate how the PD range would be affected by the parameters of the model. In fact, the effect of stimulus amplitude ϕ_n^{stim} on the PD range had been investigated in [15]. In the following, we will employ a similar method to understand the effects of parameters on PD generation.

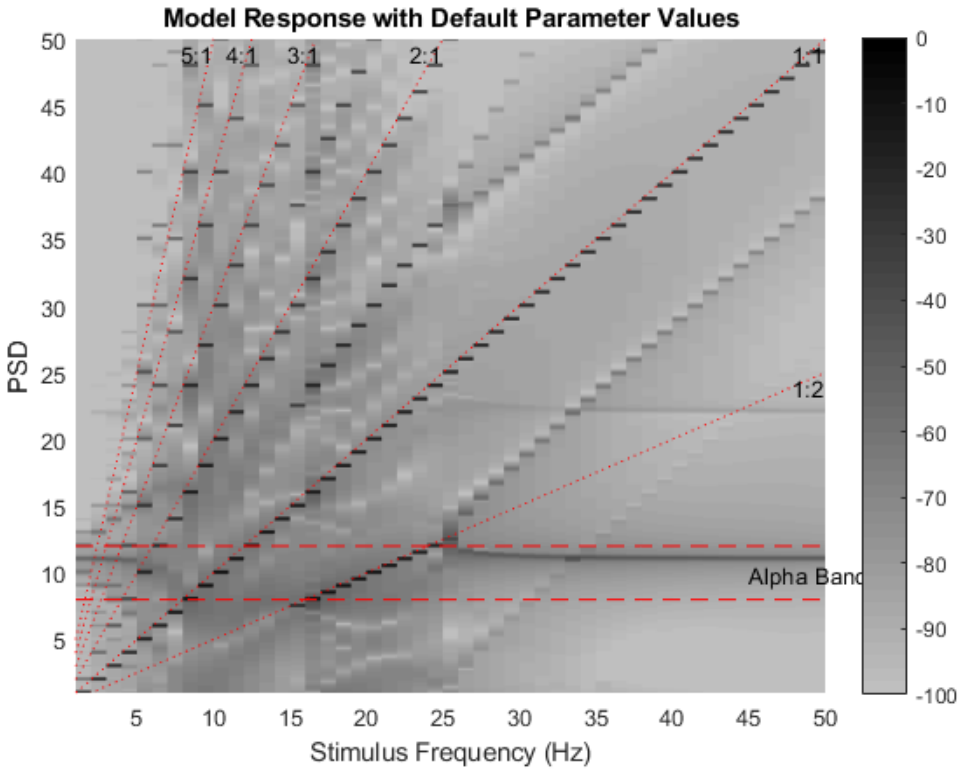

Figure 4.2: The two dimensional plot of the model responses to stimulation frequencies from 1 to 50 Hz with parameter values chosen as in Table 1. Notice that unlike the experimental plots (Figs. 3.6 and 3.7), this plot is in logarithmic scale. It can be seen that the alpha band component is being entrained to fundamental components (1:1 line) in frequencies between 5-15 Hz, and then to subharmonic components (1:2 line) in frequencies between 15-25 Hz. At other frequencies (0-5 Hz and 25-50 Hz) the power at alpha frequency (11Hz) can be seen as a horizontal gray line.

In order to distinguish such parameters, we modified the structure of the model. That is to say, (i) we cut off cortical feedback connection by setting v_{re} and v_{se} (both separately and together) to zero, or (ii) we cut off intrathalamic feedback connection by setting v_{sr} to zero, and observed thalamic and cortical outputs ϕ_s and ϕ_e respectively. We found out that regardless of whether the cortical feedback connections are cut off or not, there is subharmonic generation at both outputs as long as the intrathalamic loop is maintained. This loop is highlighted in red in

Figure 4.1. Therefore, we claim that these subharmonic oscillations are generated in the intrathalamic feedback loop.

We then focused on the effects of different parameters in this loop to subharmonic generation. The parameters in this loop are $v_{sr}, v_{rs}, v_{sn}, \alpha, \beta, \alpha_{sr}, \beta_{sr}, Q_{max}, \sigma, \theta, \phi_n^{BG}$ and ϕ_n^{stim}. We neglected v_{sn} as the same effect of would be observable when ϕ_n^{stim} is varied instead, so we are left with 11 parameters. We used a coarse grid (4 to 10 values per parameter) for the parameter spaces for the sake of simplicity. While values for a parameter is being swept, other remaining parameters are set to default values (Table 4.1).

In Figure 4.3, effects of four parameters $(\alpha, \alpha_{sr}, \phi_n^{stim}, \phi_n^{BG})$ on subharmonic generation is shown. The effects of the remaining 7 parameters are given in the appendix. From these four parameters, ϕ_n^{stim} had been previously investigated in [15]. Same results are again visible in Figure 4.3. In this case, ϕ_n^{stim} is increased from 1 to 5. When it is set to 1, the subharmonic generation seems to occur at stimulation frequencies between 20-25 Hz. As the value is increased to 5, the lower limit of this subharmonic generation interval decreases to 10, making the interval as 10-25 Hz. It is important to note that ϕ_n^{stim} does not affect the alpha oscillation. Similar observations can be made for the parameter α. As α is varied from 50 to 200, the upper limit of the subharmonic frequency interval increases. However, with default values for other parameters alpha oscillation seems to cease as α is increased. With increasing α_{sr}, it can be deduced that the subharmonic region shifts upwards while its width stays unaffected. However, at higher values (e.g. 15 or 20), it seems that many complex nonlinear interactions occur, yielding a very crowded and unrealistic spectra. For ϕ_n^{BG}, lower values affect the presence of both alpha oscillation and subharmonic components while higher values yield complicated spectra with little effect on the subharmonic interval.

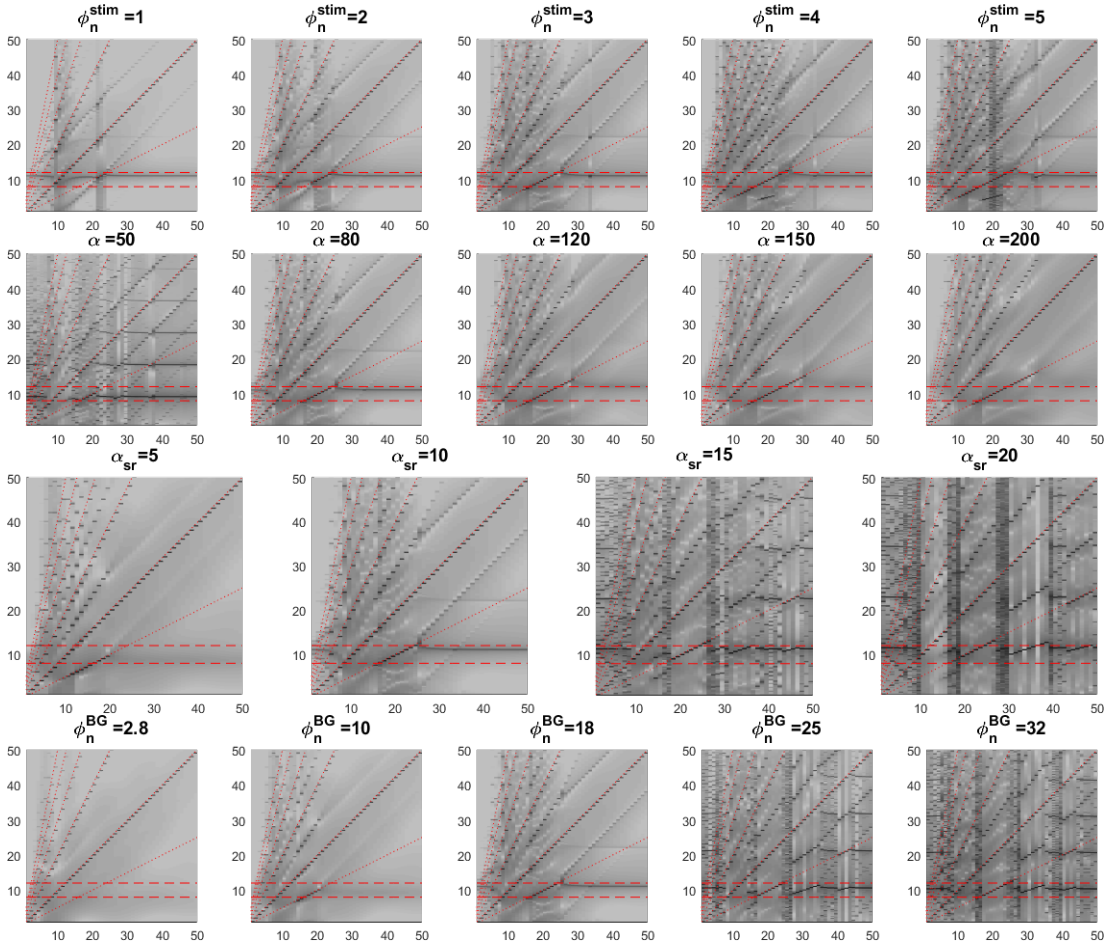

Figure 4.3: Effects of four parameters $(\alpha, \alpha_{sr}, \phi_n^{stim}, \phi_n^{BG})$ on subharmonic generation are shown. Topmost row shows model responses for$\phi_n^{stim} = 1, 2, 3, 4, 5$, second row for $\alpha = 50, 80, 120, 150, 200$, third row for $\alpha_{sr} = 5, 10, 15, 20$, and bottommost row for $\phi_n^{BG} = 2.8, 10, 18, 25, 32$. While these values are swept for the relevant parameter, the values for other parameters are selected as in Table 4.1.

These suggested us that the model is able to show very different subharmonic generation intervals for different parameter sets. We then proceeded to observe the effects of values of the parameters when they are swept together (at the same time). Taking into consideration the individual effects of all 11 parameters, we concluded not to include the input parameters ϕ_n^{stim} and ϕ_n^{BG} in this analysis because we believe that they do not reflect inherent properties of the visual system. We also considered the effects of v_{sr}, v_{rs} and Q_{max} to be weak when compared

with the effects of other parameters, so we neglected these parameters as well. Thus, we decided to only consider the six parameters ($\alpha, \beta, \alpha_{sr}, \beta_{sr}, \sigma$ and θ) and keep $v_{sr}, v_{rs}, Q_{max}, \phi_n^{stim}$ and ϕ_n^{BG} unchanged from their values in Table 4.1. In short, we searched for different subharmonic generation intervals by changing the values of the parameters $\alpha, \beta, \alpha_{sr}, \beta_{sr}, \sigma$ and θ at the same time.

Three examples of very different subharmonic generation intervals obtained after such analysis are given in Figure 4.4. In the first plot, the interval broadens from both ends and gets to be between 15-30 Hz. Notice that the so called "alpha oscillation" of the model barely escaped the 8-12 Hz alpha interval and is approximately at 13 Hz. In the second plot, the interval shifted to higher frequencies while its width remained unchanged. Similar to first plot, the "alpha oscillation" is shifted upwards outside the 8-12 Hz alpha interval. These two cases suggested that the alpha oscillation and the subharmonic interval are interrelated in some way. In the last plot, both effects in the first two plots (i.e. broadening and shifting) are merged. In this case, it seems that "alpha oscillation" is not present at all. However, possibly due to the limited amount of sweeps per parameter, we were not able to find a parameter set that would broaden the subharmonic region while keeping the alpha oscillation frequency unchanged (it either shifted upwards or totally vanished as in the plots).

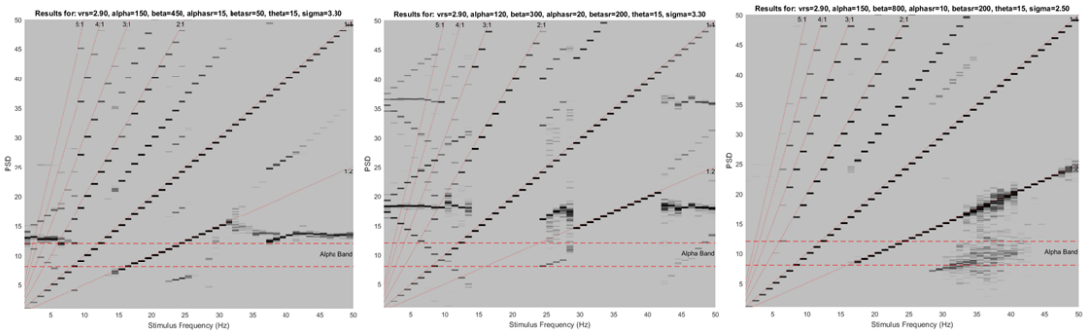

Figure 4.4: Model responses with very different subharmonic generation intervals for different parameter sets is shown. Parameters are set as follows (values for the remaining parameters are selected as in Table 4.1): In the leftmost plot $\alpha = 150, \beta = 450, \alpha_{sr} = 15, \beta_{sr} = 50, \theta = 15, \sigma = 3.3$, in the middle plot $\alpha = 120, \beta = 300, \alpha_{sr} = 20, \beta_{sr} = 200, \theta = 15, \sigma = 3.3$ and in the rightmost plot $\alpha = 150, \beta = 800, \alpha_{sr} = 10, \beta_{sr} = 200, \theta = 15, \sigma = 2.5$

We isolated the intrathalamic loop from the rest of the circuit for further analysis (Figure 4.5). Here, the loop consists of two nonlinear elements (both of the shifted sigmoidal type), two gain elements and two second order low pass filters. For such systems, it is known that constant amplitude oscillations occur if two conditions are satisfied at the frequency of interest: (i) loop gain should be unity (ii) total phase change across the loop should be 0 radians (or $2k\pi$ radians where $k = 0, 1, 2, ...$). Given that the system is driven with a signal of the form $DC + B\cos(\omega t + \phi)$, we may assume the following signal at location 1 (see bold numbers on Figure 4.5) in the loop:

$$\mathbf{1}: DC_1 + B_1\cos(\omega t + \phi_{B_1}) + A_1\cos(\frac{\omega}{2}t + \phi_{A_1}) \tag{4.22}$$

where the presence of $A_1\cos(\frac{\omega}{2}t + \phi_{A_1})$ assumes that a subharmonic oscillation is obtained through the loop. We then need to relate the signal at location 1 to the one at location 2. This is where describing function theory comes in handy, as it helps us to continue forming the loop equations as follows (also here we translate the signal to phasor representation, knowing that each component is at different frequencies):

$$\mathbf{2}: DC_1N_1(0) + B_1e^{j\phi_{B_1}}N_1(\omega) + A_1e^{j\phi_{A_1}}N_1(\frac{\omega}{2}) \tag{4.23}$$

Here N_1 stands for the describing function of the first nonlinear block in the loop. We then proceed writing the signals at each location:

$$\mathbf{3}: DC_1 N_1(0) v_{rs} + B_1 e^{j\phi_{B_1}} N_1(\omega) v_{rs} + A_1 e^{j\phi_{A_1}} N_1(\frac{\omega}{2}) v_{rs} \tag{4.24}$$

$$\mathbf{4}: DC_1 N_1(0) v_{rs} H_\alpha(0) + B_1 e^{j\phi_{B_1}} N_1(\omega) v_{rs} H_\alpha(\omega) + A_1 e^{j\phi_{A_1}} N_1(\frac{\omega}{2}) v_{rs} H_\alpha(\frac{\omega}{2}) \tag{4.25}$$

$$\mathbf{5}: DC_1 N_1(0) v_{rs} H_\alpha(0) N_2(0) + B_1 e^{j\phi_{B_1}} N_1(\omega) v_{rs} H_\alpha(\omega) N_2(\omega) + A_1 e^{j\phi_{A_1}} N_1(\frac{\omega}{2}) v_{rs} H_\alpha(\frac{\omega}{2}) N_2(\frac{\omega}{2}) \tag{4.26}$$

$$\mathbf{6}: DC_1 N_1(0) v_{rs} H_\alpha(0) N_2(0) v_{sr} + B_1 e^{j\phi_{B_1}} N_1(\omega) v_{rs} H_\alpha(\omega) N_2(\omega) v_{sr} + A_1 e^{j\phi_{A_1}} N_1(\frac{\omega}{2}) v_{rs} H_\alpha(\frac{\omega}{2}) N_2(\frac{\omega}{2}) v_{sr} \tag{4.27}$$

$$\mathbf{7}: DC_1 N_1(0) v_{rs} H_\alpha(0) N_2(0) v_{sr} H_{sr}(0) + B_1 e^{j\phi_{B_1}} N_1(\omega) v_{rs} H_\alpha(\omega) N_2(\omega) v_{sr} H_{sr}(\omega) + A_1 e^{j\phi_{A_1}} N_1(\frac{\omega}{2}) v_{rs} H_\alpha(\frac{\omega}{2}) N_2(\frac{\omega}{2}) v_{sr} H_{sr}(\frac{\omega}{2}) \tag{4.28}$$

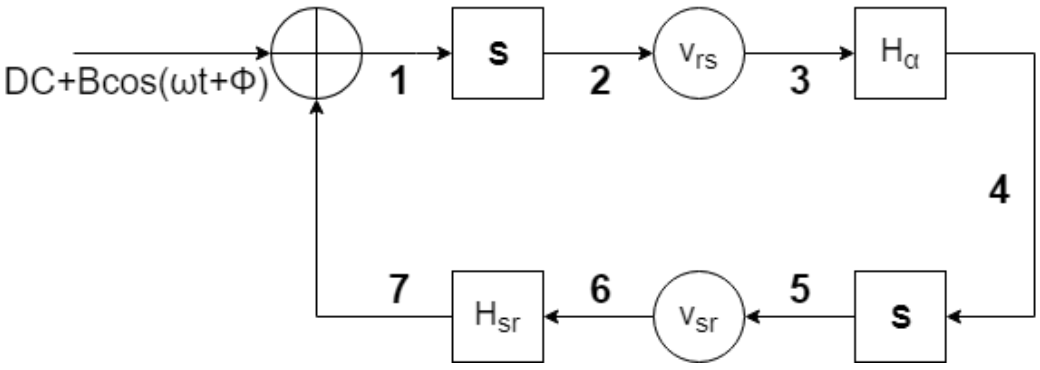

Figure 4.5: The isolated intrathalamic loop consists of two nonlinear elements (**S**), two gain elements (v_{rs} and v_{sr}) and two second order low pass filters (H_α and H_{sr}). The loop is driven with a signal of the form $DC + B\cos(\omega t + \phi)$. The bold numbers 1 to 7 are locations used in equations 4.22 to 4.28.

Then we complete the loop (location 7→location 1) and obtain 3 equations (2 are complex):

$$DC_1 N_1(0) v_{rs} H_\alpha(0) N_2(0) v_{sr} H_{sr}(0) + DC = DC_1 \tag{4.29}$$

$$B_1 e^{j\phi_{B_1}} N_1(\omega) v_{rs} H_\alpha(\omega) N_2(\omega) v_{sr} H_{sr}(\omega) + B e^{j\phi} = B_1 e^{j\phi_{B_1}} \tag{4.30}$$

$$A_1 e^{j\phi_{A_1}} N_1(\frac{\omega}{2}) v_{rs} H_\alpha(\frac{\omega}{2}) N_2(\frac{\omega}{2}) v_{sr} H_{sr}(\frac{\omega}{2}) = A_1 e^{j\phi_{A_1}} \tag{4.31}$$

For given DC, B, ϕ and ω, the above equations (5 real equations when the complex ones are separated as real and imaginary) can be solved for $DC_1, A_1, B_1, \phi_{A_1}$ and ϕ_{B_1}. This means that, we are able to judge if a parameter set will generate subharmonic oscillations without simulating the model. See Figure 4.6 for an example of an accurate solution with $DC = 30, B = 2.8, \phi = \pi/2$ and $\omega = 18Hz$. This, of course, is possible as long as the solution converges to the right solution (it may converge to a wrong solution or may not converge at all). This makes the choice of initial conditions a very critical task as it both affects the presence and speed of convergence.

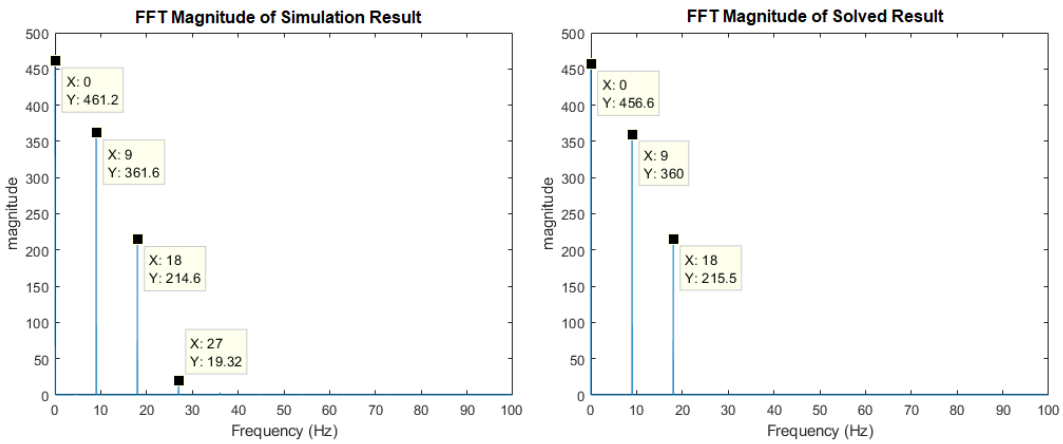

Figure 4.6: Plots showing compliance between simulation results and results from the equations. For any given DC, B, ϕ and ω, equations 4.29 to 4.31 (5 real equations when the complex ones are separated as real and imaginary) can be solved for the subharmonic magnitude and phase at any point in the loop. In this example the values are chosen as: $DC = 30, B = 2.8, \phi = \pi/2$ and $\omega = 18Hz$. Notice that the effect of the 27Hz $(3f/2)$ component is not considered while the equations were formed (due to sharp filtering characteristic of H_{sr}), hence the small differences between two results.

4.4 Discussion of Modeling Results

Given our experimental results in Figure 3.6 and Figure 3.7 and Herrmann's results [6], it becomes arguable that in the stimulation frequencies of 15-30 Hz there is subharmonic entrainment. Specifically, if subharmonic frequency falls near the alpha range of the EEG (8-15 Hz), alpha oscillation in the brain is shifted to this subharmonic frequency. This consequently means that alpha frequency and subharmonic frequency do not coexist in this stimulation interval. On the other hand, in the stimulation frequencies of 30-42 Hz (and possibly higher) subharmonic components and alpha band components tend to coexist (i.e. there is no entrainment whatsoever). However, this is not the case with the modeling results. Although the present model can show PD behaviour, the subharmonic oscillation and alpha band components do not seem to coexist in any stimulation frequency.

Thus, the model is not conforming to the above mentioned experimental observation. In other words, although the model is able to generate subharmonic frequencies, the current state is not a realistic representation of this phenomenon. Exploring possible modifications or parameter values on the model with this new dimension on constraining parameters could be a subject for a future modeling study.

We also provide a possible approach to take for doing such a modeling study by reducing the entire model to five nonlinear equations regarding subharmonic generation. This not only converts the problem to a numerical one and plants a numerical constraint on the tested parameter sets instead of an observation based constraint as expressed by [15], but may also provide a faster alternative to simulating the model in a parameter sweep study that aims at finding parameter values that would generate subharmonic oscillations at a desired frequency interval. If somehow the solution method is expedited and thus the convergence to a solution becomes short enough (e.g. shorter than it takes to complete 100 seconds of simulation time with $dt = 10^{-4}s$, these equations can be utilized as a semi-analytic parameter sweep modality. For such a study, of course, the choice of initial conditions should also be explored. In any case, this approach provides a numerical explanation as to how these subharmonic components exist in the model output.

By scrutinizing the model, we hypothesize that the observed PD behavior has its origins at the intrathalamic feedback loop. The testing of this hypothesis could be a subject of a new study with intracranial recordings taken directly from subcortical structures under a periodic light stimulus. We consider that findings of such a study would be of great importance to the factuality and authenticity of the model, regardless of those findings being parallel or anti-parallel to model predictions. As a concluding remark, we strongly believe that subharmonic oscillations are important properties of SSVEP responses, and that any modeling study regarding SSVEP responses should consider the presence of this empirically verified nonlinear behavior in the model output.

Chapter 5

Conclusion and Discussion

We have performed SSVEP experiments on 9 subjects covering stimulation frequencies in the range of 15-42 Hz. One of the major observations is that there are great inter-subject and intra-subject variability in experiments conducted on different days. Moreover, the statistical results of the repeatability experiments show PD behaviour may change in the short term. Therefore, we claim both short term effects (attention level, gaze, fatigue, etc.) and long term effects (physiological state, psychological state, etc.) may alter PD generation. These effects could be explored in further experimental studies.

Our experiments further suggested that PD may occur in all stimulation frequencies in the 15-42 Hz range. Although we did not study frequencies above 42 Hz, in the literature there are studies showing PD generation above this range, even up to 70Hz [12, 13]. In any case, an exact range in which PD occurs can not be proposed. Furthermore, when it comes to modeling studies, it is observed that they are insufficient in fully explaining and reproducing this phenomenon. In short, the insufficiency could be explained as follows:

Given the current experimental results in Figure 3.6 and Figure 3.7 and earlier experimental results [6, 12, 13], subharmonic entrainment phenomenon seems

to be present between stimulation frequencies 15-30 Hz. This means that subharmonic oscillations are in 7.5 to 15 Hz interval, which fall in the alpha band defined for EEG. This is interpreted as alpha entrainment in the sense that if subharmonic oscillation frequency falls in the alpha range and the alpha response is facilitated (hence the name "entrainment"). At frequencies higher than 30 Hz, subharmonic entrainment seems to cease and both the alpha and subharmonic oscillations take place together. On the other hand, the model predictions show that for any stimulus frequency these two oscillations can not be generated together. This happens for different parameter sets. Thus, we claim that the current model employed to explain the PD behavior can not sufficiently predict the brain responses regarding subharmonic oscillations. It may be conjectured that, perhaps, this insufficiency can be overcome by simple parameter adjustments. We have tried to identify the effects of parameter values on the PD phenomenon by doing some rather narrow scoped parameter sweeps. However, we could not overcome this insufficiency by changing the parameter values, possibly due to the coarse grid we employed for the parameter spaces. Exploring the 17 dimensional parameter space is not a trivial task as such exploration requires extensive memory, computational power and time. A detailed sweep could also be a basis for a future work. Even such a parameter sweep study may not be able to see cases in which alpha and subharmonic oscillations are seen together. Therefore, in any case, the mechanism of entrainment should be investigated similar to what we did for subharmonic generation. We have also showed that the range of stimulation frequencies for which subharmonic oscillations are generated is controllable by parameters in the model. Therefore, although we observed different ranges in experimental and modeling studies, we do not consider this difference to be a misfit between the experimental and modeling results and consequently this is not an insufficiency of the model.

The anatomical and physiological mechanisms underlying the subharmonic oscillations are still unknown. We hypothesize from our modeling results that the subharmonic responses originate in the thalamus, particularly the intrathalamic loop in the model. This hypothesis could be experimentally tested with invasive subcortical recordings.

Other modeling studies that we have found in the literature regarding the SSVEP responses have not focused on subharmonic generations. Our studies however, clearly indicate that, subharmonic generation should be considered as an important property of the SSVEP response. Therefore, we claim that in future studies, investigators should consider the validity of this behavior in the model output. Similar argument was also suggested and considered beneficial to modeling literature by Roberts in [15].

In earlier studies [12, 81, 82], PD occurrences were found in electroretinogram (ERG) recordings. Consequently, an experimental study that simultaneously records ERG and EEG could give insight on the origins of this phenomenon. This is important because in our modeling work we assumed these oscillations are solely generated in the brain and thus neglected the role of the retina. If in such experiment it is found that PD could be present in EEG while it is absent in ERG, our results and ideas regarding the origins of PD would be strongly backed up.

A key task in modeling work is to observe the behaviour of the model under different parameter values. With nonlinear models, such as the one in the current study, this often requires a new simulation for each parameter set. We believe a possible contribution of this study to further modeling studies is in this regard. The entire model was reduced to five nonlinear equations regarding subharmonic generation. These, when solved with a nonlinear solver, determine whether there will be a subharmonic oscillation at the model output or not. In this way, the need for simulating the model could potentially be replaced by this semi-analytic approach, and future parameter sweep studies could employ this approach when PD behaviour is being considered.

As a final point, we also suggest that SSVEP based BCIs could potentially benefit from the presence of subharmonic oscillations in SSVEP responses. This is because in our experimental results we have observed subharmonic peaks that are much larger in amplitude than fundamental peaks, which would otherwise confuse the classifier. Incorporating subharmonic oscillations into the classifier is therefore likely to improve the performances of SSVEP based BCIs.

Bibliography

[1] D. Regan, "Some characteristics of average steady-state and transient responses evoked by modulated light," *Electroencephalography and Clinical Neurophysiology*, vol. 20, no. 3, pp. 238–248, 1966.

[2] D. Regan, *Human brain electrophysiology: evoked potentials and evoked magnetic fields in science and medicine*. Elsevier, 1989.

[3] G. Bin, X. Gao, Z. Yan, B. Hong, and S. Gao, "An online multi-channel ssvep-based brain computer interface using a canonical correlation analysis method," *Journal of Neural Engineering*, vol. 6, p. 046002, Mar 2009.

[4] R. Ortner, B. Z. Allison, G. Korisek, H. Gaggl, and G. Pfurtscheller, "An ssvep bci to control a hand orthosis for persons with tetraplegia," *IEEE Transactions on Neural Systems and Rehabilitation Engineering*, vol. 19, no. 1, pp. 1–5, 2011.

[5] F.-B. Vialatte, M. Maurice, J. Dauwels, and A. Cichocki, "Steady-state visually evoked potentials: Focus on essential paradigms and future perspectives," *Progress in Neurobiology*, vol. 90, no. 4, pp. 418–438, 2010.

[6] C. S. Herrmann, "Human eeg responses to 1-100hz flicker: resonance phenomena in visual cortex and their potential correlation to cognitive phenomena," *Experimental Brain Research*, vol. 137, pp. 346–353, Feb 2001.

[7] P. L. Nunez, *Neocortical dynamics and human EEG rhythms*. Oxford University Press, 1995.

[8] A. M. Norcia, L. G. Appelbaum, J. M. Ales, B. R. Cottereau, and B. Rossion, "The steady-state visual evoked potential in vision research: A review," *Journal of Vision*, vol. 15, p. 4, May 2015.

[9] G. Rager and W. Singer, "The response of cat visual cortex to flicker stimuli of variable frequency," *European Journal of Neuroscience*, vol. 10, no. 5, pp. 1856–1877, 1998.

[10] L. H. Tweel and H. Spekreijse, "Signal transport and rectification in the human evoked-response system," *Annals of the New York Academy of Sciences*, vol. 156, no. 2 Rein Control,, pp. 678–695, 1969.

[11] R. Townsend, A. Lubin, and P. Naitoh, "Stabilization of alpha frequency by sinusoidally modulated light," *Electroencephalography and Clinical Neurophysiology*, vol. 39, no. 5, pp. 515–518, 1975.

[12] D. W. Crevier and M. Meister, "Synchronous period-doubling in flicker vision of salamander and man," *Journal of Neurophysiology*, vol. 79, no. 4, pp. 1869–1878, 1998.

[13] T. Tsoneva, G. Garcia-Molina, and P. Desain, "Neural dynamics during repetitive visual stimulation," *Journal of Neural Engineering*, vol. 12, no. 6, p. 066017, 2015.

[14] M. Labecki, R. Kus, A. Brzozowska, T. Stacewicz, B. S. Bhattacharya, and P. Suffczynski, "Nonlinear origin of ssvep spectra?a combined experimental and modeling study," *Frontiers in Computational Neuroscience*, vol. 10, 2016.

[15] J. Roberts and P. Robinson, "Quantitative theory of driven nonlinear brain dynamics," *NeuroImage*, vol. 62, no. 3, pp. 1947–1955, 2012.

[16] A. Spiegler, *Dynamics of biologically informed neural mass models of the brain*. Univ.-Verl., 2011.

[17] S. Laureys and G. Tononi, *The Neurology of Consciousness*. Academic Press, 2009.

[18] S. Baillet, J. Mosher, and R. Leahy, "Electromagnetic brain mapping," *IEEE Signal Processing Magazine*, vol. 18, no. 6, pp. 14–30, 2001.

[19] A. B. Usakli, "Improvement of eeg signal acquisition: An electrical aspect for state of the art of front end," *Computational Intelligence and Neuroscience*, vol. 2010, pp. 1–7, 2010.

[20] C. Fonseca, J. P. S. Cunha, R. E. Martins, V. M. Ferreira, J. P. M. D. Sa, M. A. Barbosa, and A. M. D. Silva, "A novel dry active electrode for eeg recording," *IEEE Transactions on Biomedical Engineering*, vol. 54, no. 1, pp. 162–165, 2007.

[21] B. A. Taheri, R. T. Knight, and R. L. Smith, "A dry electrode for eeg recording," *Electroencephalography and Clinical Neurophysiology*, vol. 90, no. 5, pp. 376–383, 1994.

[22] A. Kübler, B. Kotchoubey, J. Kaiser, J. R. Wolpaw, and N. Birbaumer, "Brain-computer communication: Unlocking the locked in.," *Psychological Bulletin*, vol. 127, no. 3, pp. 358–375, 2001.

[23] B. Anand, G. Chhina, and B. Singh, "Some aspects of electroencephalographic studies in yogis," *Electroencephalography and Clinical Neurophysiology*, vol. 13, no. 3, pp. 452–456, 1961.

[24] L. Aftanas and S. Golocheikine, "Human anterior and frontal midline theta and lower alpha reflect emotionally positive state and internalized attention: high-resolution eeg investigation of meditation," *Neuroscience Letters*, vol. 310, no. 1, pp. 57–60, 2001.

[25] T. Fernandez, T. Harmony, M. Rodriguez, J. Bernal, J. Silva, A. Reyes, and E. Marosi, "Eeg activation patterns during the performance of tasks involving different components of mental calculation," *Electroencephalography and Clinical Neurophysiology*, vol. 94, no. 3, pp. 175–182, 1995.

[26] J. B. Caplan, J. R. Madsen, S. Raghavachari, and M. J. Kahana, "Distinct patterns of brain oscillations underlie two basic parameters of human maze learning," *Journal of Neurophysiology*, vol. 86, no. 1, pp. 368–380, 2001.

[27] J. A. Pineda, "The functional significance of mu rhythms: Translating ?seeing? and ?hearing? into ?doing?," *Brain Research Reviews*, vol. 50, no. 1, pp. 57–68, 2005.

[28] W. Klimesch, "Eeg-alpha rhythms and memory processes," *International Journal of Psychophysiology*, vol. 26, no. 1-3, pp. 319–340, 1997.

[29] A. Black, "The operant conditioning of central nervous system electrical activity," *Psychology of Learning and Motivation*, pp. 47–95, 1972.

[30] L. Venables and S. H. Fairclough, "The influence of performance feedback on goal-setting and mental effort regulation," *Motivation and Emotion*, vol. 33, no. 1, pp. 63–74, 2009.

[31] G. Pfurtscheller and C. Neuper, "Motor imagery and direct brain-computer communication," *Proceedings of the IEEE*, vol. 89, no. 7, pp. 1123–1134, 2001.

[32] K.-H. Lee, L. M. Williams, M. Breakspear, and E. Gordon, "Synchronous gamma activity: a review and contribution to an integrative neuroscience model of schizophrenia," *Brain Research Reviews*, vol. 41, no. 1, pp. 57–78, 2003.

[33] P. Brown, S. Salenius, J. C. Rothwell, and R. Hari, "Cortical correlate of the piper rhythm in humans," *Journal of Neurophysiology*, vol. 80, no. 6, pp. 2911–2917, 1998.

[34] W. Lutzenberger, F. Pulvermüller, T. Elbert, and N. Birbaumer, "Visual stimulation alters local 40-hz responses in humans: an eeg-study," *Neuroscience Letters*, vol. 183, no. 1-2, pp. 39–42, 1995.

[35] M. M. Müller, A. Keil, T. Gruber, and T. Elbert, "Processing of affective pictures modulates right-hemispheric gamma band eeg activity," *Clinical Neurophysiology*, vol. 110, no. 11, pp. 1913–1920, 1999.

[36] M. MuLler, J. Bosch, T. Elbert, A. Kreiter, M. Sosa, P. Sosa, and B. Rockstroh, "Visually induced gamma-band responses in human electroencephalographic activity a link to animal studies," *Experimental Brain Research*, vol. 112, no. 1, 1996.

[37] H. G. Vaughan, "The relationship of brain activity to scalp recordings of event-related potentials.," *Average evoked potentials: Methods, results, and evaluations.*, pp. 45–94, 1969.

[38] G. Dawson, "A summation technique for the detection of small evoked potentials," *Electroencephalography and Clinical Neurophysiology*, vol. 6, pp. 65–84, 1954.

[39] J. V. Odom, M. Bach, C. Barber, M. Brigell, M. F. Marmor, A. P. Tormene, and G. E. Holder, "Visual evoked potentials standard (2004)," *Documenta Ophthalmologica*, vol. 108, no. 2, pp. 115–123, 2004.

[40] J. Yin, D. Jiang, and J. Hu, "Design and application of brain-computer interface web browser based on vep," *2009 International Conference on Future BioMedical Information Engineering (FBIE)*, 2009.

[41] E. Basar, T. Demiralp, M. Schürmann, C. Basar-Eroglu, and A. Ademoglu, "Oscillatory brain dynamics, wavelet analysis, and cognition," *Brain and Language*, vol. 66, no. 1, pp. 146–183, 1999.

[42] N. R. Galloway, "Human brain electrophysiology: Evoked potentials and evoked magnetic fields in science and medicine," *British Journal of Ophthalmology*, vol. 74, pp. 255–255, Jan 1990.

[43] J. D. Victor and J. Mast, "A new statistic for steady-state evoked potentials," *Electroencephalography and Clinical Neurophysiology*, vol. 78, no. 5, pp. 378–388, 1991.

[44] A. Gelb and V. d. V. W. E., *Multiple-input describing functions and nonlinear system design*. McGraw-Hill, 1968.

[45] J. C. West and J. L. Douce, "The mechanism of sub-harmonic generation in a feedback system," *Proceedings of the IEE - Part B: Radio and Electronic Engineering*, vol. 102, no. 5, pp. 569–574, 1955.

[46] T. Wang, "Analyzing Oscillators using Describing Functions," *ArXiv e-prints*, Sept. 2017.

[47] A. Mcintosh, "Towards a network theory of cognition," *Neural Networks*, vol. 13, no. 8-9, pp. 861–870, 2000.

[48] S. L. Bressler and J. Kelso, "Cortical coordination dynamics and cognition," *Trends in Cognitive Sciences*, vol. 5, no. 1, pp. 26–36, 2001.

[49] S. L. Bressler, "Understanding cognition through large-scale cortical networks," *Current Directions in Psychological Science*, vol. 11, no. 2, pp. 58–61, 2002.

[50] V. K. Jirsa, "Connectivity and dynamics of neural information processing," *Neuroinformatics*, vol. 2, no. 2, pp. 183–204, 2004.

[51] A. L. Hodgkin and A. F. Huxley, "Propagation of electrical signals along giant nerve fibres," *Proceedings of the Royal Society B: Biological Sciences*, vol. 140, no. 899, pp. 177–183, 1952.

[52] J. A. S. Kelso, *Dynamic patterns: the self-organization of brain and behavior*. MIT Press, 2000.

[53] E. P. Hoel, L. Albantakis, and G. Tononi, "Quantifying causal emergence shows that macro can beat micro," *Proceedings of the National Academy of Sciences*, vol. 110, no. 49, pp. 19790–19795, 2013.

[54] P. L. Nunez and R. Srinivasan, *Electric fields of the brain: the neurophysics of EEG*. Oxford University Press, 2006.

[55] G. Deco, V. K. Jirsa, P. A. Robinson, M. Breakspear, and K. Friston, "The dynamic brain: From spiking neurons to neural masses and cortical fields," *PLoS Computational Biology*, vol. 4, no. 8, 2008.

[56] V. K. Jirsa and H. Haken, "Field theory of electromagnetic brain activity," *Physical Review Letters*, vol. 77, no. 5, pp. 960–963, 1996.

[57] P. A. Robinson, C. J. Rennie, and J. J. Wright, "Propagation and stability of waves of electrical activity in the cerebral cortex," *Physical Review E*, vol. 56, pp. 826–840, Jan 1997.

[58] S. Coombes, N. A. Venkov, L. Shiau, I. Bojak, D. T. J. Liley, and C. R. Laing, "Modeling electrocortical activity through improved local approximations of integral neural field equations," *Physical Review E*, vol. 76, Jan 2007.

[59] M. Breakspear, "Dynamic models of large-scale brain activity," *Nature Neuroscience*, vol. 20, no. 3, pp. 340–352, 2017.

[60] W. J. Freeman, *Mass action in the nervous system: examination of the neurophysiological basis of adaptive behavior through the EEG*. Acad. Press, 1975.

[61] C. J. Honey, R. Kotter, M. Breakspear, and O. Sporns, "Network structure of cerebral cortex shapes functional connectivity on multiple time scales," *Proceedings of the National Academy of Sciences*, vol. 104, pp. 10240–10245, Apr 2007.

[62] G. Deco, V. Jirsa, A. R. Mcintosh, O. Sporns, and R. Kotter, "Key role of coupling, delay, and noise in resting brain fluctuations," *Proceedings of the National Academy of Sciences*, vol. 106, pp. 10302–10307, Mar 2009.

[63] P. A. Robinson, C. J. Rennie, and D. L. Rowe, "Dynamics of large-scale brain activity in normal arousal states and epileptic seizures," *Physical Review E*, vol. 65, Nov 2002.

[64] F. Freyer, J. A. Roberts, R. Becker, P. A. Robinson, P. Ritter, and M. Breakspear, "Biophysical mechanisms of multistability in resting-state cortical rhythms," *Journal of Neuroscience*, vol. 31, no. 17, pp. 6353–6361, 2011.

[65] M. Breakspear, J. A. Roberts, J. R. Terry, S. Rodrigues, N. Mahant, and P. A. Robinson, "A unifying explanation of primary generalized seizures

through nonlinear brain modeling and bifurcation analysis," *Cerebral Cortex*, vol. 16, pp. 1296–1313, Sep 2005.

[66] A. Phillips and P. Robinson, "A quantitative model of sleep-wake dynamics based on the physiology of the brainstem ascending arousal system," *Journal of Biological Rhythms*, vol. 22, no. 2, pp. 167–179, 2007.

[67] F. L. D. Silva, "Neural mechanisms underlying brain waves: from neural membranes to networks," *Electroencephalography and Clinical Neurophysiology*, vol. 79, no. 2, pp. 81–93, 1991.

[68] A. C. Marreiros, J. Daunizeau, S. J. Kiebel, and K. J. Friston, "Population dynamics: Variance and the sigmoid activation function," *NeuroImage*, vol. 42, no. 1, pp. 147–157, 2008.

[69] K.-F. Wong, "A recurrent network mechanism of time integration in perceptual decisions," *Journal of Neuroscience*, vol. 26, no. 4, pp. 1314–1328, 2006.

[70] M. Breakspear, L. M. Williams, and C. J. Stam, "A novel method for the topographic analysis of neural activity reveals formation and dissolution of dynamic cell assemblies," *Journal of Computational Neuroscience*, vol. 16, no. 1, pp. 49–68, 2004.

[71] K. E. Stephan, L. Kamper, A. Bozkurt, G. A. P. C. Burns, M. P. Young, and R. Kotter, "Advanced database methodology for the collation of connectivity data on the macaque brain (cocomac)," *Philosophical Transactions of the Royal Society B: Biological Sciences*, vol. 356, no. 1412, pp. 1159–1186, 2001.

[72] S. Horvät, R. Gamanut, M. Ercsey-Ravasz, L. Magrou, B. Gamanut, D. C. V. Essen, A. Burkhalter, K. Knoblauch, Z. Toroczkai, H. Kennedy, and et al., "Spatial embedding and wiring cost constrain the functional layout of the cortical network of rodents and primates," *PLOS Biology*, vol. 14, no. 7, 2016.

[73] V. Jirsa and H. Haken, "A derivation of a macroscopic field theory of the brain from the quasi-microscopic neural dynamics," *Physica D: Nonlinear Phenomena*, vol. 99, no. 4, pp. 503–526, 1997.

[74] P. A. Robinson, P. N. Loxley, S. C. O'Connor, and C. J. Rennie, "Modal analysis of corticothalamic dynamics, electroencephalographic spectra, and evoked potentials," *Physical Review E*, vol. 63, no. 4, 2001.

[75] C. J. Rennie, P. A. Robinson, and J. J. Wright, "Unified neurophysical model of eeg spectra and evoked potentials," *Biological Cybernetics*, vol. 86, pp. 457–471, Jan 2002.

[76] F. H. L. D. Silva, A. Hoeks, H. Smits, and L. H. Zetterberg, "Model of brain rhythmic activity," *Kybernetik*, vol. 15, no. 1, pp. 27–37, 1974.

[77] W. C. Wang, "Optical detectors," 2011.

[78] D. C. Howell, *Statistical methods for psychology*. Thomson Wadsworth, 8th ed., 2012.

[79] Y. J. Kim, M. Grabowecky, K. A. Paller, K. Muthu, and S. Suzuki, "Attention induces synchronization-based response gain in steady-state visual evoked potentials," *Nature Neuroscience*, vol. 10, no. 1, pp. 117–125, 2006.

[80] T. Cao, F. Wan, C. Wong, J. D. Cruz, and Y. Hu, "Objective evaluation of fatigue by eeg spectral analysis in steady-state visual evoked potential-based brain-computer interfaces," *BioMedical Engineering OnLine*, vol. 13, no. 1, p. 28, 2014.

[81] M. R. Shah, K. R. Alexander, H. Ripps, and H. Qian, "Characteristics of period doubling in the rat cone flicker erg," *Experimental Eye Research*, vol. 90, no. 2, pp. 196–202, 2010.

[82] K. R. Alexander, M. W. Levine, and B. J. Super, "Characteristics of period doubling in the human cone flicker electroretinogram," *Visual Neuroscience*, vol. 22, no. 06, pp. 817–824, 2005.

[83] M. Carandini, "Do we know what the early visual system does?," *Journal of Neuroscience*, vol. 25, no. 46, pp. 10577–10597, 2005.

[84] D. A. Kaiser, "Cortical cartography," *Biofeedback*, vol. 38, no. 1, pp. 9–12, 2010.

[85] Q. Liu, K. Chen, Q. Ai, and S. Q. Xie, "Review: Recent development of signal processing algorithms for ssvep-based brain computer interfaces," *Journal of Medical and Biological Engineering*, vol. 34, pp. 299–309, Jan 2014.

[86] S. Amiri, A. Rabbi, L. Azinfar, and R. Fazel-Rezai, "A review of p300, ssvep, and hybrid p300/ssvep brain- computer interface systems," *Brain-Computer Interface Systems - Recent Progress and Future Prospects*, May 2013.

[87] B. H. Jansen and V. G. Rit, "Electroencephalogram and visual evoked potential generation in a mathematical model of coupled cortical columns," *Biological Cybernetics*, vol. 73, pp. 357–366, Jan 1995.

[88] Y. Tuncel, T. Başaklar, and Y. Z. Ider, "Period doubling behavior in human steady state visual evoked potentials," *Biomedical Physics & Engineering Express*, vol. 4, p. 025024, Feb 2018.

[89] F. L. D. Silva and W. S. V. Leeuwen, "The cortical source of the alpha rhythm," *Neuroscience Letters*, vol. 6, no. 2-3, pp. 237–241, 1977.

[90] P. Robinson, C. Rennie, D. Rowe, and S. Oconnor, "Estimation of multiscale neurophysiologic parameters by electroencephalographic means," *Human Brain Mapping*, vol. 23, no. 1, pp. 53–72, 2004.

Appendix A

Parameter Sweep Results of $v_{sr}, v_{rs}, \beta, \beta_{sr}, Q_{max}, \sigma, \theta$

In Figure A.1, effects of the remaining seven parameters ($v_{sr}, v_{rs}, \beta, \beta_{sr}, Q_{max}, \sigma, \theta$) on subharmonic generation is shown. In all these plots, default values are used for parameters other than the swept parameter. As β is increased from 150 to 2000, subharmonic regime tends to slowly shift from 10-20 Hz to 15-25 Hz, keeping its width pretty much unchanged. The alpha oscillation frequency shifts from 8Hz to 12Hz as β is increased (power at alpha components seems to drop as is β increased). For lower values of β, the spectrum becomes very crowded and complex, possibly owing to many nonlinear interactions taking effect. For values β¿800, the spectrum remains largely unaffected (only change seems to be the decreasing power at alpha band) from increasing β. As β_{sr} is varied from 10 to 200, the subharmonic regime shifts upwards (i.e. 5-15 Hz to 25-35 Hz) with decreasing power at this regime (at β_{sr}=200, the subharmonic components are barely distinguishable from background). The native oscillation frequency (f_α) also shifts upwards with the subharmonic regime, going outside the alpha band. The effects of increasing Q_{max} is not as impactful as other parameters. The position of the subharmonic regime is unaffected, while its width is barely affected at the upper limit (the interval changed from 15-24 Hz to 15-25 Hz). The power of the alpha oscillation seems to increase as Q_{max} increases with its frequency fairly

unaffected. σ is arguably the most influential parameter on the subharmonic regime. For lower values ($\sigma = 2, 2.5$) , the spectrum is utterly cluttered, with lots of nonlinear components including many higher order subharmonics. For higher values of σ, both the subharmonic regime and alpha oscillation vanish, only leaving the fundamental and harmonic components in the spectrum. θ significantly affects the width of the subharmonic regime. As it is varied from 10 to 25, subharmonic regime first extends from the upper limit then from the lower limit (at $\theta = 20$ the width is doubled). After $\theta = 20$, the regime tends to shift downwards with vanishing power at alpha oscillation. For $v_{rs} = 0.2$, subharmonic regime is inexistent. For increasing v_{rs} values, the width of the regime is subtly affected at the upper limit, but the alpha oscillation frequency shifts upwards, from 10Hz to 12Hz. Higher values for v_{sr}, kill off both the subharmonic components and the alpha oscillation (as expected due to negative feedback). At lower values, subharmonic regime seems to be faintly affected by v_{sr} while alpha oscillation seems to cease as v_{sr} is increased from 0.2 to 1.5.

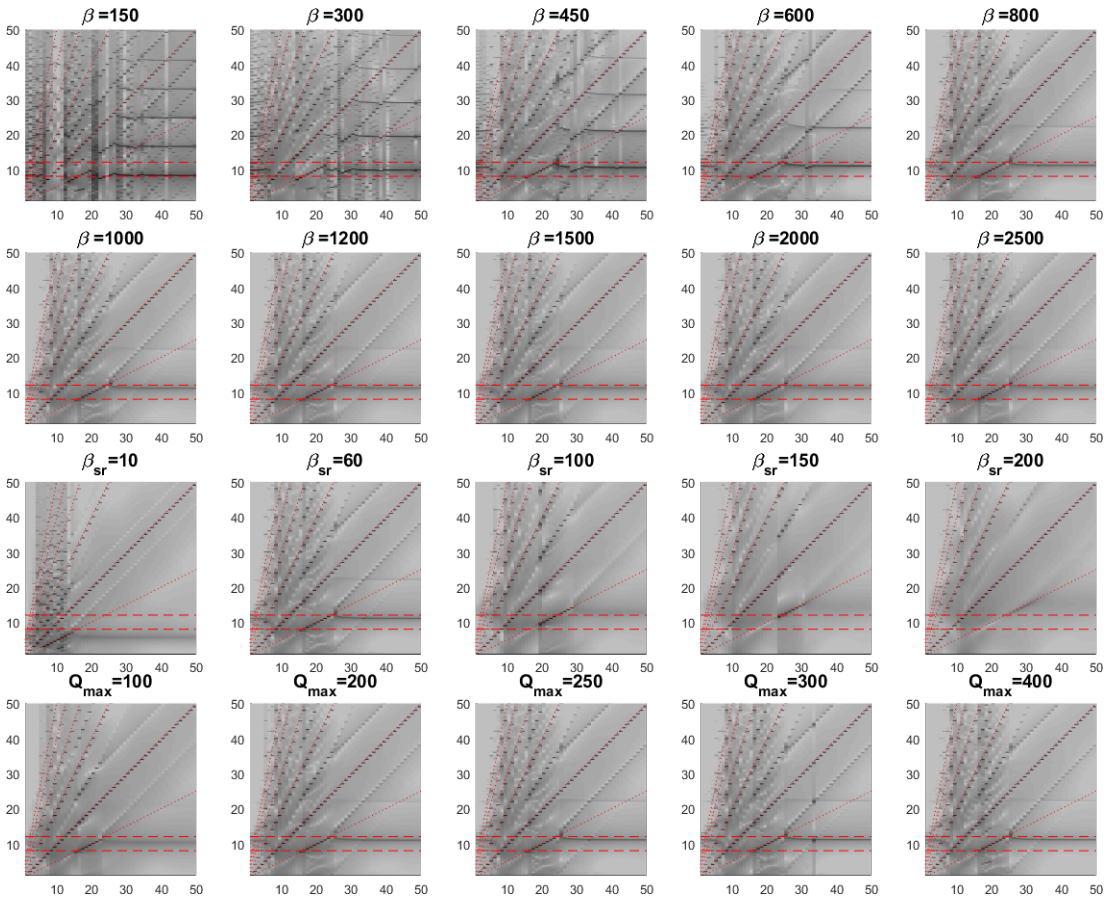

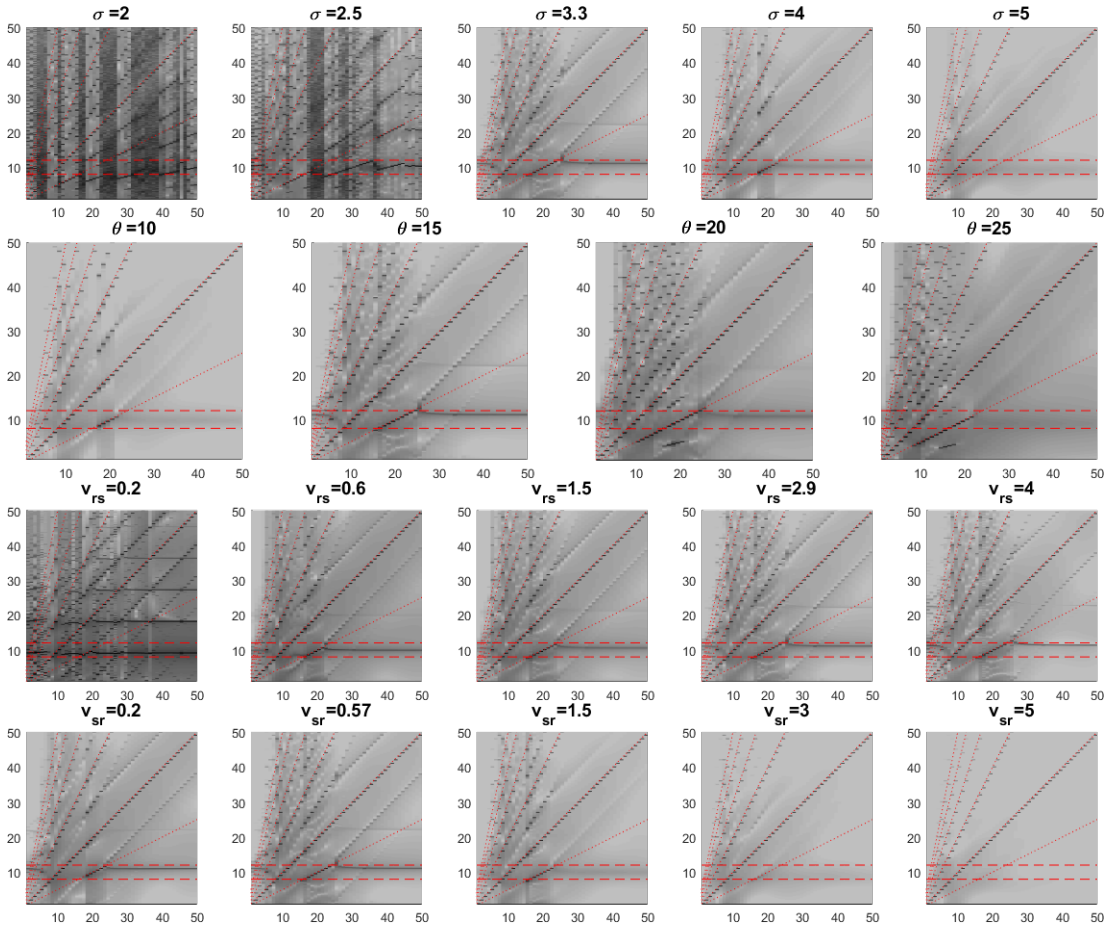

Figure A.1: Effects of seven $(v_{sr}, v_{rs}, \beta, \beta_{sr}, Q_{max}, \sigma, \theta)$ different parameters on subharmonic generation are shown. Two topmost rows show model responses for $\beta = 150, 300, 450, 600, 800, 1000, 1200, 1500, 2000, 2500$, third row for $\beta_{sr} = 10, 60, 100, 150, 200$, fourth row for $Q_{max} = 100, 200, 250, 300, 400$, fifth row for $\sigma = 2, 2.5, 3.3, 4, 5$, fifth row for $\theta = 10, 15, 20, 25$, sixth row for $v_{rs} = 0.2, 0.6, 1.5, 2.9, 4$, and bottommost row for $v_{sr} = 0.2, 0.57, 1.5, 3, 5$. While these values are swept for the relevant parameter, the values for other parameters are selected as in Table 4.1.

Appendix B

Data Gathered in Short Term Repeatability Experiments

Table B.1: SORc values of each stimulation frequency in 5 consecutive repeatability experiments for S2. First column lists the stimulation frequencies used in all 5 experiments. Second to sixth columns list the corresponding SORc values in different experiments.

Stimulus Frequency	**Exp1**	**Exp2**	**Exp3**	**Exp4**	**Exp5**
25Hz	17%	0%	0%	17%	0%
26Hz	17%	0%	33%	100%	100%
27Hz	17%	17%	0%	33%	67%
28Hz	67%	0%	17%	100%	67%
29Hz	17%	50%	0%	0%	67%
30Hz	0%	50%	83%	100%	83%
31Hz	67%	33%	100%	83%	50%
32Hz	0%	100%	50%	100%	100%
33Hz	0%	83%	50%	50%	0%
34Hz	0%	100%	17%	100%	67%
35Hz	100%	17%	0%	100%	100%

Table B.2: Average SORe values for each stimulation frequency in O and P channels for S2. First column lists the stimulation frequencies used in all 5 experiments. Second column lists the average of the SORe values of O1,Oz,O2 channels. Third column lists the average of the SORe values of P3,Pz,P4 channels

Stimulus Frequency	**Oavg**	**Pavg**
25Hz	13%	0%
26Hz	47%	53%
27Hz	47%	7%
28Hz	47%	53%
29Hz	33%	20%
30Hz	60%	67%
31Hz	67%	67%
32Hz	60%	80%
33Hz	47%	27%
34Hz	53%	60%
35Hz	60%	67%
Avg.	48%	45%

Table B.3: SORc values of each stimulation frequency in 5 consecutive repeatability experiments for S4. First column lists the stimulation frequencies used in all 5 experiments. Second to sixth columns list the corresponding SORc values in different experiments.

Stimulus Frequency	**Exp1**	**Exp2**	**Exp3**	**Exp4**	**Exp5**
25Hz	17%	0%	0%	17%	0%
26Hz	17%	0%	33%	100%	100%
27Hz	17%	17%	0%	33%	67%
28Hz	67%	0%	17%	100%	67%
29Hz	17%	50%	0%	0%	67%
30Hz	0%	50%	83%	100%	83%
31Hz	67%	33%	100%	83%	50%
32Hz	0%	100%	50%	100%	100%
33Hz	0%	83%	50%	50%	0%
34Hz	0%	100%	17%	100%	67%
35Hz	100%	17%	0%	100%	100%

Table B.4: Average SORe values for each stimulation frequency in O and P channels for S4. First column lists the stimulation frequencies used in all 5 experiments. Second column lists the average of the SORe values of O1,Oz,O2 channels. Third column lists the average of the SORe values of P3,Pz,P4 channels

Stimulus Frequency	**Oavg**	**Pavg**
25Hz	73%	67%
26Hz	33%	20%
27Hz	13%	33%
28Hz	33%	40%
29Hz	33%	27%
30Hz	20%	33%
31Hz	7%	40%
32Hz	40%	27%
33Hz	13%	20%
34Hz	73%	53%
35Hz	47%	47%
Avg.	35%	37%

Table B.5: SORc values of each stimulation frequency in 5 consecutive repeatability experiments for S7. First column lists the stimulation frequencies used in all 5 experiments. Second to sixth columns list the corresponding SORc values in different experiments.

Stimulus Frequency	**Exp1**	**Exp2**	**Exp3**	**Exp4**	**Exp5**
25Hz	0%	0%	100%	17%	17%
26Hz	0%	50%	100%	0%	100%
27Hz	0%	33%	67%	83%	83%
28Hz	33%	33%	17%	33%	67%
29Hz	100%	0%	33%	0%	17%
30Hz	33%	17%	67%	17%	0%
31Hz	83%	50%	17%	67%	0%
32Hz	0%	50%	17%	50%	0%
33Hz	50%	0%	33%	0%	17%
34Hz	0%	17%	33%	17%	33%
35Hz	0%	17%	0%	17%	83%

Table B.6: Average SORe values for each stimulation frequency in O and P channels for S7. First column lists the stimulation frequencies used in all 5 experiments. Second column lists the average of the SORe values of O1,Oz,O2 channels. Third column lists the average of the SORe values of P3,Pz,P4 channels

Stimulus Frequency	**Oavg**	**Pavg**
25Hz	27%	27%
26Hz	53%	47%
27Hz	67%	40%
28Hz	27%	47%
29Hz	27%	33%
30Hz	27%	27%
31Hz	33%	53%
32Hz	20%	27%
33Hz	13%	27%
34Hz	13%	27%
35Hz	27%	20%
Avg.	30%	34%

Table B.7: SORc values of each stimulation frequency in 5 consecutive repeatability experiments for S8. First column lists the stimulation frequencies used in all 5 experiments. Second to sixth columns list the corresponding SORc values in different experiments.

Stimulus Frequency	**Exp1**	**Exp2**	**Exp3**	**Exp4**	**Exp5**
25Hz	0%	0%	0%	17%	67%
26Hz	33%	17%	0%	0%	0%
27Hz	17%	17%	0%	17%	0%
28Hz	0%	0%	0%	67%	33%
29Hz	0%	0%	67%	0%	100%
30Hz	17%	17%	0%	0%	0%
31Hz	50%	0%	0%	17%	50%
32Hz	17%	0%	17%	0%	50%
33Hz	0%	0%	83%	0%	67%
34Hz	33%	0%	0%	0%	17%
35Hz	100%	17%	0%	33%	0%

Table B.8: Average SORe values for each stimulation frequency in O and P channels for S8. First column lists the stimulation frequencies used in all 5 experiments. Second column lists the average of the SORe values of O1,Oz,O2 channels. Third column lists the average of the SORe values of P3,Pz,P4 channels

Stimulus Frequency	**Oavg**	**Pavg**
25Hz	20%	13%
26Hz	0%	20%
27Hz	7%	13%
28Hz	27%	13%
29Hz	33%	33%
30Hz	7%	7%
31Hz	33%	13%
32Hz	7%	27%
33Hz	33%	27%
34Hz	7%	13%
35Hz	40%	20%
Avg.	19%	18%